Available online at www.sciencedirect.com
ScienceDirect
ELSEVIER
Deep-Sea Research II 53 (2006) 2808–2832
DEEP-SEA RESEARCH PART II
www.elsevier.com/locate/dsr2

Influence of model geometrical fitting and turbulence parameterization on phytoplankton simulation in the Gulf of Maine

Rucheng Tian*, Changsheng Chen

Department of Fisheries Oceanography, School for Marine Science and Technology, University of Massachusetts Dartmouth, 838 South Rodney French Blvd., New Bedford, MA 02744, USA

Accepted 31 August 2006
Available online 13 November 2006

Abstract

Numerical experiments were made to examine the influences of model geometrical fitting and turbulence parameterization on the temporal and spatial distributions of simulated phytoplankton in the Gulf of Maine. The assessment of the role of geometrical fitting was made by running a state-of-the-art Nutrient-Phytoplankton-Zooplankton (NPZ) model with physical fields provided from unstructured-grid, finite-volume coastal ocean model (FVCOM) and structured-grid, finite-difference coastal ocean model (ECOM-si), respectively. The impact of turbulence parameterization was studied by running a coupled NPZ–FVCOM system with various vertical turbulence modules implemented in the General Ocean Turbulence Model (GOTM). Comparisons were focused on three large tidal dissipation regions: Georges Bank (characterized by strong tidal rectification over steep bottom topography and tidal mixing fronts), Bay of Fundy (featuring large semidiurnal tidal oscillations due to the gulf-scale resonance), and Nantucket Shoals (a tidal energy flux convergence zone). For the same given tidal forcing and initial physical and biological conditions, the ability of a model to accommodate the irregular coastal geometry and steep bottom topography is critical in determining the robustness of the simulated spatial and temporal structure of N and P. For the same given external forcing in FVCOM, turbulence parameterizations have less impact on N and P in mixed regions than in stratified regions. In mixed regions, both q–ε and q–ql models reproduced the observed vertical mixing intensity. Since biological variables remained vertically mixed in these regions, their structures were little affected by turbulence closure schemes. In stratified regions, q–ε models predicted stronger mixing than q–ql models, which produced more nutrient fluxes over the slope and thus influenced the growth and distribution of P around the tidal mixing front. A direct comparison between observed and model-predicted turbulence dissipation rates suggests that q–ε models with a mixing cutoff at Richardson number of 1.0 predict more realistic mixing intensity than q–ql models in stratified regions on Georges Bank.

Keywords: Phytoplankton dynamics; Tidal mixing front; Geometrical fitting; Physical–biological modeling; Gulf of Maine

1. Introduction

Due to near-resonance geometry and complex topography, the Gulf of Maine (GoM) is

*Corresponding author. Tel.: +1 508 910 6383; fax: +1 508 910 6342.
E-mail addresses: rtian@umassd.edu (R. Tian), c1chen@umassd.edu (C. Chen).

0967-0645/$ - see front matter © 2006 Elsevier Ltd. All rights reserved.
doi:10.1016/j.dsr2.2006.08.006

characterized by strong tide-driven hydrodynamics. Three sub-regions are of particular importance in terms of tidal energy dissipation and rectification: the Bay of Fundy (BF), Georges Bank (GB), and Nantucket Shoals (NS). Semidiurnal tidal waves propagate into the GoM mainly through the northeastern boundary (Fig. 1). Most of the tidal energy enters into the BF, generating a high tidal elevation ranging from 8 to 16 m (Garrett, 1972, 1974; Greenberg, 1979), forming a major tidal energy dissipation zone in the GoM. NS, southeast of Nantucket Island (NI), is characterized by strong tidal mixing. A recent modeling study by Chen et al. (2006a) revealed that the southeastern side of NS is an area of energetic interaction between two tidal waves, one propagating southward along the Cape Cod coast and the other northeastward from the southern New England shelf. Strong nonlinear interaction between these two out-of-phase tidal waves creates a zone of low sea-surface level and high tidal energy dissipation in the adjacent area (Chen et al., 2006a). Over GB, the tidal current exceeds 100 cm/s (Chen et al., 2001). The nonlinear interaction between tidal currents and steep bottom topography generates a clockwise residual gyre around the bank (Loder, 1980; Butman et al., 1982; Loder and Wright, 1985; Limeburner and Beardsley, 1989; Chen and Beardsley, 1995). This residual gyre is intensified during spring and summer as the tidal mixing front develops (Chen et al., 1995; Naimie, 1996). The tidal mixing front is generated by the variation of vertical mixing intensity with depth due to stratification. In summer, it is a closed round-bank feature located at the 40-m isobath on the northern flank and the 50–60-m isobaths on the southern flank (Flagg, 1987; Chen and Beardsley, 1998). In winter, the water stratification is significantly eroded due to surface cooling. As a result, the tidal mixing front moves to the 100-m isobath and merges with the

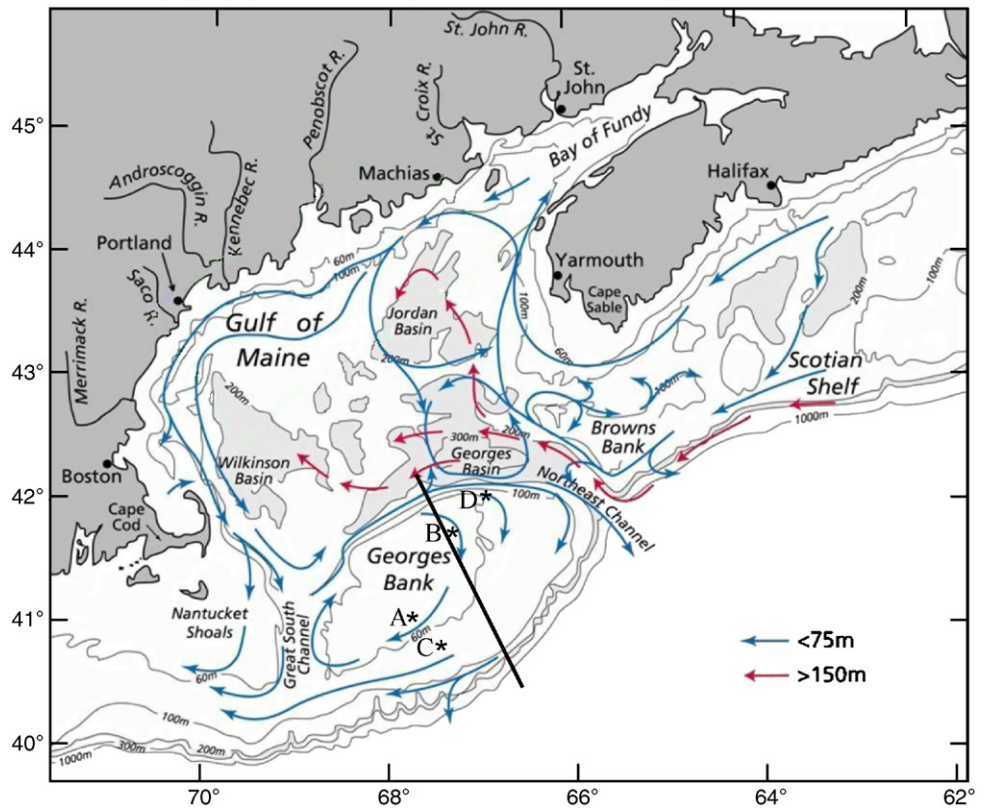

Fig. 1. Summertime general subtidal circulation pattern in the Gulf of Maine and over Georges Bank (Beardsley et al., 1997); picture provided by Robert Beardsley. The solid line indicates the position of the cross-bank transect selected to show the vertical distribution of physical and biological variables. A (41.13°N, 67.75°W) and B (41.71°N, 67.49°W) indicate the sites of in-situ microstructure measurements in the vertically mixed regions and C (40.86°N, 67.54°W) and D (42.12°N, 67.04°W) in the stratified regions on GB (Horne et al., 1996; Burgett et al., 2001).

shelf-break density front on the southern flank (Chen, 1992).

GB is one of the most biologically productive regions in the world ocean, with maximum primary production on the order of $400\,g\,C\,m^{-2}\,yr^{-1}$ (O'Reilly et al., 1987). Phytoplankton production on GB is characterized by two bloom seasons: one usually occurs in early spring and the other in summer after the tidal mixing front is established (Horne et al., 1989; Franks and Chen, 1996, 2001; Townsend and Thomas, 2002). The summer bloom is believed to be fueled by nutrient replenishment along the edges of the bank due to tidal mixing (Horne et al., 1989; Franks and Chen, 1996, 2001).

Many efforts have been made to explore the physical and biological processes controlling the formation and suppression of phytoplankton on GB and in the adjacent regions (e.g. Franks and Chen, 1996, 2001, Ji et al., 2006a, b; Townsend and Thomas, 2002). While coupled 3D physical–biological models are commonly used to study this region, the influences of the physical model's skill on the biological simulations have rarely been assessed. Based on sensitivity analysis, Broström (2002) pointed out that coarse horizontal resolutions could overestimate the horizontal advection of biological state variables and thus degrade biological simulations. He suggested that the grid resolution of a General Circulation Model (GCM) must be $<8\,km$ to simulate adequately phytoplankton advection in the open ocean. Similar results were obtained by Oschlies (2002) and Moll and Radach (2003). Coastal oceans are characterized by bays, inlets and estuaries with complex, irregular geometry and steep bottom topography. Recent model comparison experiments conducted by Chen et al. (2006b) suggested that resolving the geometry was critical to providing an accurate simulation of circulation, stratification and mixing on GB, BF and NS in the GoM. Since the spatial distribution and temporal variation of phytoplankton in the GoM are closely related to advection and mixing processes, we examine here the sensitivity of a biological model to geometrical fitting in a given physical environment.

Turbulence parameterization is one of the most uncertain features in both physical and biological models. The Mellor and Yamada level-2.5 (MY2.5) turbulence closure scheme has been used widely in the coastal ocean (Mellor and Yamada, 1982). In the MY2.5 model, the vertical eddy viscosity is calculated by solving the turbulence kinetic energy and turbulence macroscale equations. This scheme seems to work well for tidal-induced mixing in shallow waters (Chen and Beardsley, 1998), but more validation is needed for stratified regions. Since vertical diffusion is one of the key processes for nutrient supply to the euphotic zone in stratified regions and no turbulence model has been proven to work reliably for stratified environments in the GoM, the uncertainty due to various turbulence parameterizations should be taken into account in the assessment of the reliability of a biological model.

In this paper we present two numerical experiments conducted in the GoM: Experiment A, focusing on influences of geometrical fitting on phytoplankton simulation; and Experiment B, studying impacts of turbulence parameterization on phytoplankton simulation. Experiment A was carried out through comparisons of Nutrient–Phytoplankton–Zooplankton (NPZ) model results under physical environments predicted by FVCOM and ECOM-si. FVCOM is an unstructured-grid finite-volume model developed by Chen et al. (2003), while ECOM-si is a structured-grid finite-difference model developed originally by Blumberg and Mellor (1987). FVCOM and ECOM-si are built on the same hydrodynamic principles but use different grid configuration and numerical methods to solve the governing equations. The unstructured triangular grid used in FVCOM provides a more accurate representation of the irregular coastal geometry and steep bottom topography, while the curvilinear grid used in ECOM-si is inflexible in resolving the complex geometry in coastal areas. Running two models under the same physical forcing allows us to examine the role of coastal geometry and steep bottom topography in phytoplankton simulations in the GoM.

Experiment B was conducted by running FVCOM with various turbulence closure modules implemented in the General Ocean Turbulence Model (GOTM) (Burchard et al., 1999). The q–ε (q: turbulence kinetic energy and ε: the turbulence dissipation rate) and q–ql (l: macroscale) turbulence models were assessed by a direct comparison between model-predicted and observed turbulence dissipation rates in mixed and stratified regions on GB. The impacts of turbulence parameterizations on nutrient transport and growth of phytoplankton were then examined.

2. Method

2.1. Physical models

FVCOM is a prognostic, unstructured-grid, finite-volume, free-surface, 3D primitive-equation ocean circulation model developed by Chen et al. (2003). FVCOM consists of momentum, continuity, temperature, salinity and density equations, and is closed physically and mathematically with a default setup of the Mellor and Yamada level-2.5 turbulence closure scheme for vertical mixing and the Smagorinsky turbulence closure scheme for horizontal mixing (Smagorinsky, 1963). The governing equations in FVCOM are discretized using an unstructured triangular grid in the horizontal and the σ-coordinate transformation in the vertical. The triangular grid has the advantage of resolving complex coastal geometry, and the terrain-following vertical coordinates provide a better representation of irregular bottom topography. FVCOM is solved numerically using the 2nd-order finite-volume flux discrete scheme through a split-mode approach (Chen et al., 2004). The sea-surface elevation is calculated in the external mode composed of the two-dimensional (2D) vertically averaged momentum and continuity equations while the 3D currents, salinity and temperature are computed in the internal mode composed of the 3D governing equations with the sea-surface pressure gradient force from the external mode. A transport adjustment is made between external and internal modes to ensure volume conservation in individual control volumes at each time step. This finite-volume approach combines the best of finite-element methods for geometric flexibility and finite-difference methods for simple discrete structures and computational efficiency. The flux calculation methods used in FVCOM guarantee the volume and mass conservation in each individual control volume and thus the entire computational domain, even in coastal and estuarine regions with complex irregular geometry. The updated structure of FVCOM was described in detail in Chen et al. (2006c).

ECOM-si is a semi-implicit version of the prognostic, structured grid, finite-volume 3D primitive-equation Princeton Ocean Model (POM) developed originally by Blumberg and Mellor (1987). The governing equations used for this model are the same as those of FVCOM but the numerical methods of the discretization are different. ECOM-si is discretized with a curvilinear grid in the horizontal and the σ-coordinate in the vertical. It incorporates the modified Mellor–Yamada level-2.5 turbulence closure scheme to calculate vertical eddy viscosity (Mellor and Yamada, 1982; Galperin et al., 1988) and the Smagorinsky turbulence closure scheme to parameterize horizontal diffusivity (Smagorinsky, 1963). Unlike POM and FVCOM, ECOM-si is integrated numerically through a single mode approach with a semi-implicit scheme developed by Casulli (1990). The time step used in ECOM-si is roughly equivalent to the internal mode time step used in FVCOM. A detailed description of the GoM ECOM-si model was given in Chen et al. (2001).

2.2. Turbulence models

The GOTM is a community turbulence module developed by Burchard et al. (1999) and continuously upgraded by a team effort led by Burchard (http://www.gotm.net). This module contains two types of turbulence models: (1) q–ql equations and (2) q–ε equations. Both turbulence model groups include the original code with a Richardson number cut off at 0.2 and a modified version with a Richardson number cut off between 0.2 and 1.0 (Mellor and Yamada, 1982; Kantha and Clayson, 1994; Burchard and Baumert, 1995; Burchard and Bolding, 2001; Canuto et al., 2001). GOTM is coupled to FVCOM through an interface library and different turbulence modules in GOTM can be directly selected to replace the default setup of the MY2.5 turbulence closure scheme. A detailed description of the implementation of GOTM in FVCOM was given in the FVCOM User Manual (Chen et al., 2004).

The turbulence closure schemes reside in the stability functions parameterizing the pressure–strain correlation terms of the Reynolds stress (Burchard and Bolding, 2001). Of the five terms of pressure–strain effects (isotropy, shear production, buoyancy production, non-isotropic contribution and vorticity contribution), each stability function considers a different approximate balance. We have explored five different stability functions: the modified MY2.5 stability function, which only contains isotropy and shear productions (Mellor and Yamada, 1982; Galperin et al., 1988); the Kantha–Clayson (KC) stability function, which includes both isotropic and non-isotropic contributions (Kantha and Clayson, 1994); the Burchard–

Baumert (BB) stability function, which contains the isotropy shear and buoyancy turbulence productions (Burchard and Baumert, 1995); the Canuto A (CA) stability function, which includes all five pressure–strain terms; and the Canuto B (CB) stability function, which has been deduced for an equilibrium state in which turbulence dissipation balances turbulence productions (Burchard and Bolding, 2001; Canuto et al., 2001). The MY2.5 and the KC stability functions were implemented in the q–ql and the other three stability functions were used in the q–ε equation models.

ECOM-si is closed mathematically using only q–ql equations with a modified MY 2.5 turbulence closure scheme, while FVCOM includes all the five different turbulence models described above. This was one of the reasons why Experiment B was conducted only using FVCOM in this study. For comparison between FVCOM and ECOM-si in Experiment A, both models used MY 2.5 only.

2.3. Biological model

The biological model is the NPZ model developed initially by Franks et al. (1986) for ecosystem studies in the GoM/GB region. Nitrogen is used as the tracer of state variables. Nutrient uptake is formulated by the Michaelis–Menten kinetics, while zooplankton grazing on phytoplankton is parameterized by the Ivlev functional response. The governing equation of the NPZ model is given as

$$\frac{dP}{dt} = \frac{V_m N}{k_s + N} f(I_0, z)P - ZR_m(1 - e^{-\lambda P}) - \varepsilon P, \quad (1)$$

$$\frac{dZ}{dt} = \gamma ZR_m(1 - e^{-\lambda P}) - gZ, \quad (2)$$

$$\frac{dN}{dt} = -\frac{V_m N}{k_s + N} f(I_0, z)P - (1 - \gamma)ZR_m \times (1 - e^{-\lambda P}) + \varepsilon P + gZ, \quad (3)$$

where P, Z and N are phytoplankton, zooplankton and nitrogen in $\mu mol\,N\,l^{-1}$. There are seven controlling parameters: maximal phytoplankton growth rate V_m ($2.0\,d^{-1}$), half-saturation constant k_s ($1.0\,\mu mol\,N\,l^{-1}$), zooplankton maximal grazing rate R_m ($0.5\,d^{-1}$), exponential Ivlev constant λ ($(\mu mol\,N\,l^{-1})^{-1}$), assimilation efficiency γ (0.7 dimensionless), phytoplankton mortality ε ($0.1\,d^{-1}$), zooplankton mortality g ($0.1\,d^{-1}$) and light attenuation coefficient k_{ext} (0.065–$0.1\,m^{-1}$). The parameter values used in Experiments A and B are adopted from Franks and Chen (2001). In the model, the unassimilated fraction of grazing (1–γ) and mortalities of both phytoplankton and zooplankton are considered to be recycled into dissolved nutrients. The dependence of phytoplankton growth on incident irradiance in the water column is parameterized as

$$f(I_0, z) = I_0 e^{k_{ext} z}, \quad (4)$$

where k_{ext} is the attenuation coefficient for irradiance, z is the water depth, which is positive in the upward direction, and I_0 is the normalized surface light intensity taken as a constant value of 1 in space and time (Franks and Chen, 2001). Following Franks and Chen (2001), the attenuation coefficient is given as a function of the total water depth h in the form of

$$k_{ext} = 0.065 + (0.1 - 0.065)\{1 - \tanh[(h - 80/40)]\}/2. \quad (5)$$

This function was specified to mimic the spatial variation of light attenuation due to high resuspension and phytoplankton biomass over GB and in coastal regions (Franks and Chen, 2001). This NPZ model includes the sinking of phytoplankton in the water column, specified as $1.0\,m\,d^{-1}$.

2.4. Numerical experiments

The simulation domain covered the GoM/GB region and was enclosed by an open boundary from New Jersey to the Nova Scotia shelf (Figs. 2 and 3). The FVCOM unstructured grid contained 59,949 non-overlapping triangular cells with 32,420 nodes. Higher grid resolution was used over the slope where bottom topography is steep and in the inner shelf region where coastal geometry is complex (Fig. 2) The horizontal resolution was ~0.3 km in the inner southern New England shelf and the GoM coastal areas, ~1.0–2.0 km around the shelf-break region of GB, 2–3 km over the top of GB, ~0.5–4 km in the BF and ~10 km in the interior of the GoM and in the deep region near the open boundary. The grid was built along the coastline to capture the complex geometric variation along the coast and islands.

Two orthogonal curvilinear coordinate grids were used for ECOM-si in Experiment A (Fig. 3). In the first, or "low-resolution", grid, the horizontal resolution varied from 2–4 km over GB to 4–20 km near the open boundary (Fig. 3a). In BF, the horizontal resolution is ~4 km in the cross-bay

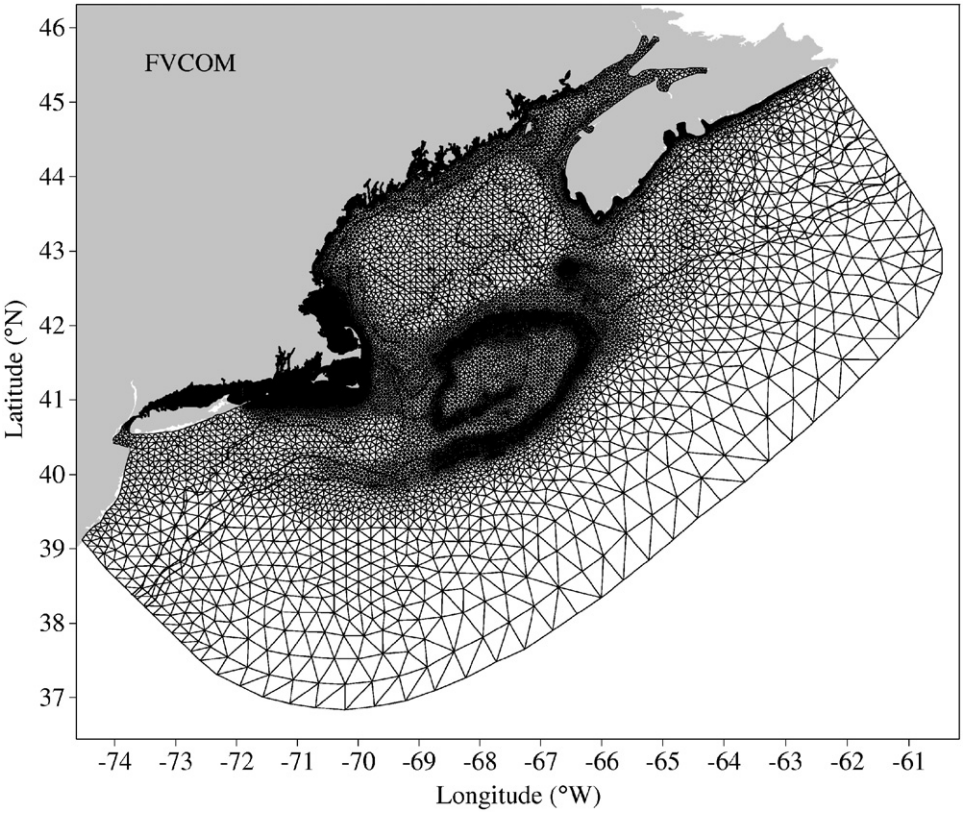

Fig. 2. Unstructured triangular grid of FVCOM in the computational domain. There are 59,949 unoverlapped triangular cells with a resolution ranging from ~0.3–1 km on South New England Shelf, ~1–2 km on the edges of Georges Bank to ~10 km in the deep region at the open boundary.

direction and ~8 km in the along-bay direction. The second, or "high-resolution", grid was generated by doubling the horizontal resolution used in the low-resolution grid (Fig. 3b). There were 19,370 grid points in the low-resolution grid and 76,368 in the high-resolution grid.

The water depth at each model grid point was interpolated directly from the USGS bathymetric database. In the open-ocean region connected to the open boundary, the water depth was cut off at 300 m to simplify the numerical treatment of the radiation open boundary condition. Both FVCOM and ECOM-si were configured with 31 σ-levels in the vertical, which provided a vertical resolution of ~1.3–4 m on GB and the shelf where the water depth was less than 120 m, and 10 m in the open ocean region where the water depth was cut off at 300 m.

To provide an objective assessment, we ran FVCOM and ECOM-si with the same initial conditions and external forcing. At the initialization, water temperature was assumed to be distributed linearly in the vertical, from 15 °C at the surface to 6 °C at the depth of 300 m. No salinity contribution was considered in the experiments as it was simply assigned to a value of 35 PSU everywhere in the entire domain. The initial conditions for N, P and Z were specified using an analytical steady-state solution of the NPZ equations derived by Franks and Chen (1996) based on the summertime conditions in the interior of the GoM (Fig. 4). Note that these idealized initial conditions only represent an average of the basic physical and biological structures in the GoM. Careful consideration must be given to our assumptions before application of the model results for interpretation of field observations.

The models were forced by the M_2 tidal elevation along the open boundary. The amplitudes and phases of the M_2 tidal elevation at each open boundary grid point were interpolated directly from the global $0.5^\circ \times 0.5^\circ$ inverse tidal model of Egbert et al. (1994), with calibration to provide the best match with the observed tidal elevations and

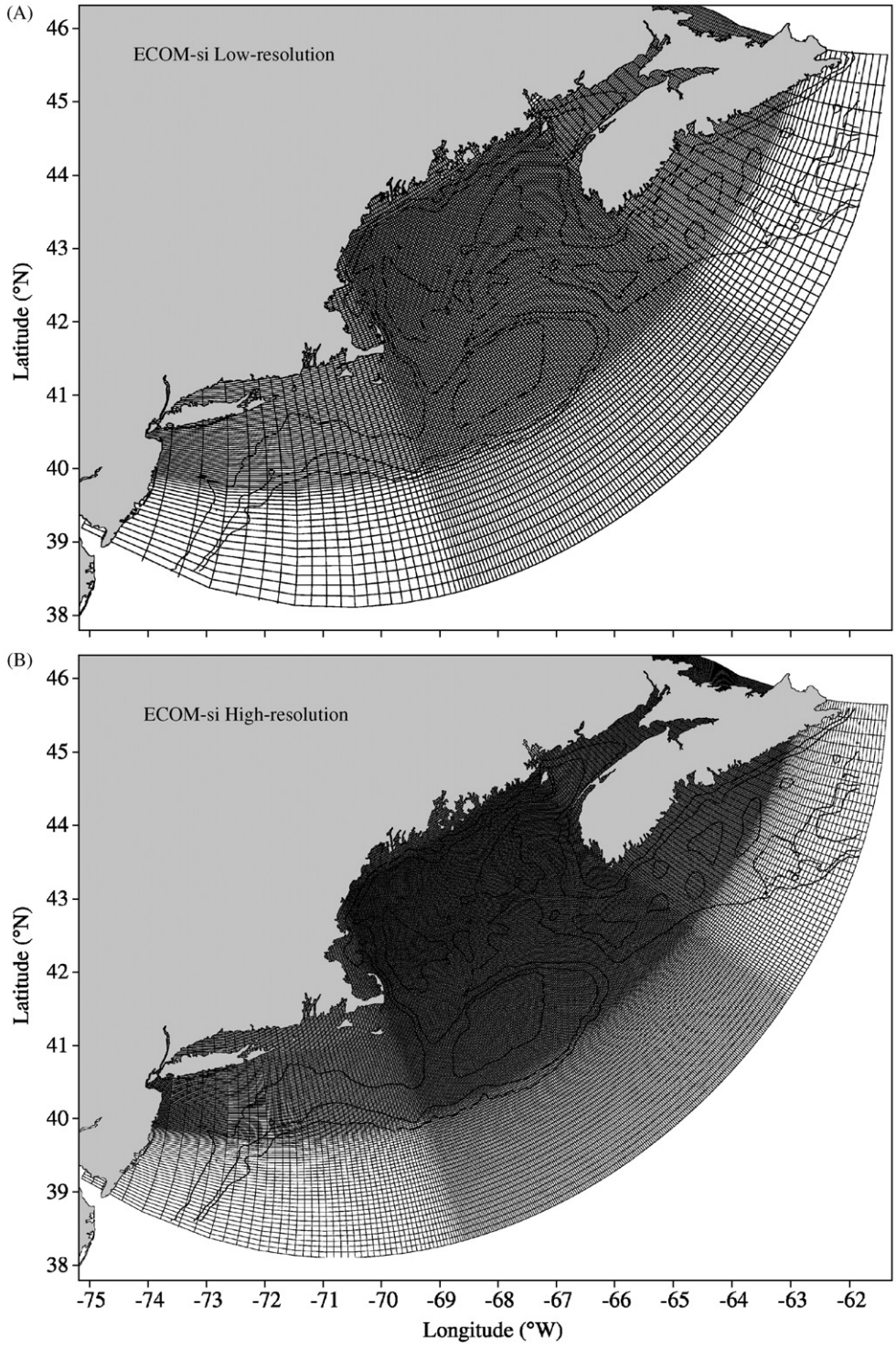

Fig. 3. Orthogonal curvilinear grid of ECOM-si. The coarse-resolution grid (upper panel) includes 19,370 grid points with a resolution ranging between ~2 km over Georges Bank and ~20 km at the open boundary. The high-resolution grid has 76,923 grid points with a resolution of ~1 km over Georges Bank and ~10 km at the open boundary.

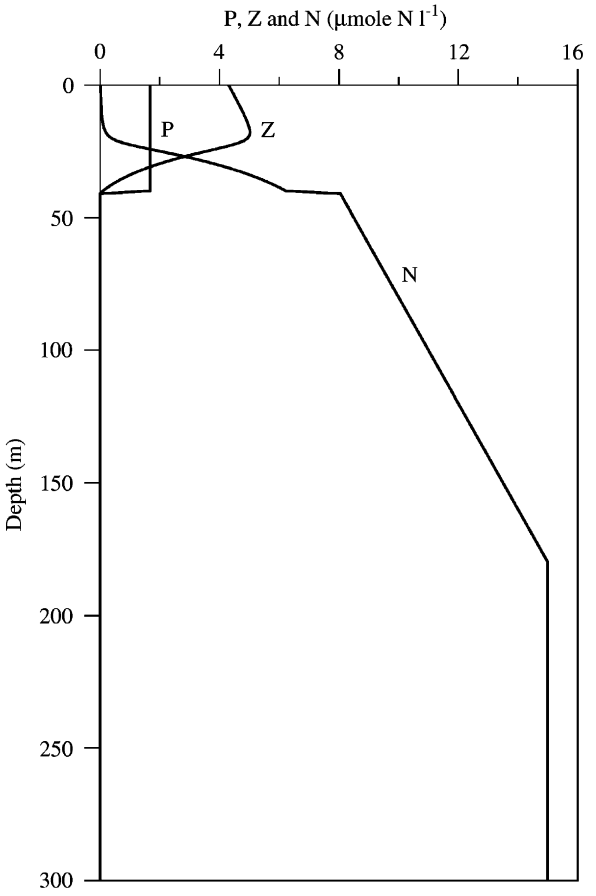

Fig. 4. Vertical profiles of nitrogen (N), phytoplankton (P) and zooplankton (Z) at the initialization. These profiles were derived by Franks and Chen (1996) for a summertime steady-state solution of the NPZ model.

currents at available tidal gauges and moorings (Chen et al., 2001, 2006b). A gravity wave radiation condition on current was applied at the open boundary to minimize energy reflection (Chen et al., 2001). A no-gradient condition was used for water temperature at the open boundary, which worked well for this case of linearly-distributed water temperature in the vertical. In all experiments, no surface heating/cooling, wind stress or river discharges were included.

The time step was set to 124.2 s for ECOM-si, which corresponded to 360 time steps over one M_2 tidal cycle (12.42 h). Because the horizontal resolution in the Nantucket Sound area was only about 300–500 m, FVCOM used 4.14 s for the external mode and 41.4 s for the internal mode, which is equivalent to 1080 time steps over one M_2 tidal cycle for the internal-mode computation. Both FVCOM and ECOM-si showed that the residual flow field and biological variables reached a quasi-equilibrium state after 20 tidal cycles. For this reason, all experiments were made for a 20-tidal-cycle model run. FVCOM is coded in Fortran 90 with Message Passing Interface (MPI) parallelization so that it can run efficiently on a multi-processor computer. ECOM-si is written in Fortran 77, which was run on a single processor 3.2 GHz Linux workstation.

3. Results

3.1. Experiment A: comparison between FVCOM and ECOM-si simulations

For the same given initial vertical stratification and tidal forcing, FVCOM and ECOM-si showed broadly similar spatial patterns of phytoplankton biomass, nitrogen concentration, nitrogen uptake rate and *f*-ratio on GB and on NS. Both models predicted high phytoplankton concentration patches within the tidal mixing frontal zone along the 60-m isobath running from Nantucket Sound to the Great South Channel (GSC) and around GB (Fig. 5). The simulated phytoplankton biomass was particularly high on the northeast peak of GB and on the northeastern edge of Nantucket Sound and Shoals. The models also suggested relatively high phytoplankton biomass at the shelf-break along the 100- to 200-m isobaths on the southern flank of GB and a low phytoplankton biomass zone between the shelf-break edge and the tidal mixing front (Fig. 5).

Both FVCOM and ECOM-si predicted a donut-like pattern of nutrient distribution on GB. Nutrient concentration was high on the northeast peak and the southwestern flank connected to the GSC and low on the crest of GB (Fig. 5). The models also showed relatively high concentration of nutrients at the western slope of the GSC. Similarly, the simulated nutrient uptake rate and *f*-ratio showed high values along the 60-m isobath on GB and over the slope of Nantucket Sound and Nantucket Shoals, with the highest values on the northeast peak of GB. Uptake rate and *f*-ratio were relatively low in the mixed region on the top of GB and also in the region between the tidal mixing front and the shelf-break edge on the southern flank of GB.

Both models predicted similar vertical distributions of nutrients and phytoplankton on GB. On the cross-bank transect shown in Fig. 1, for example, both models showed that phytoplankton were vertically well mixed on the top of GB where the

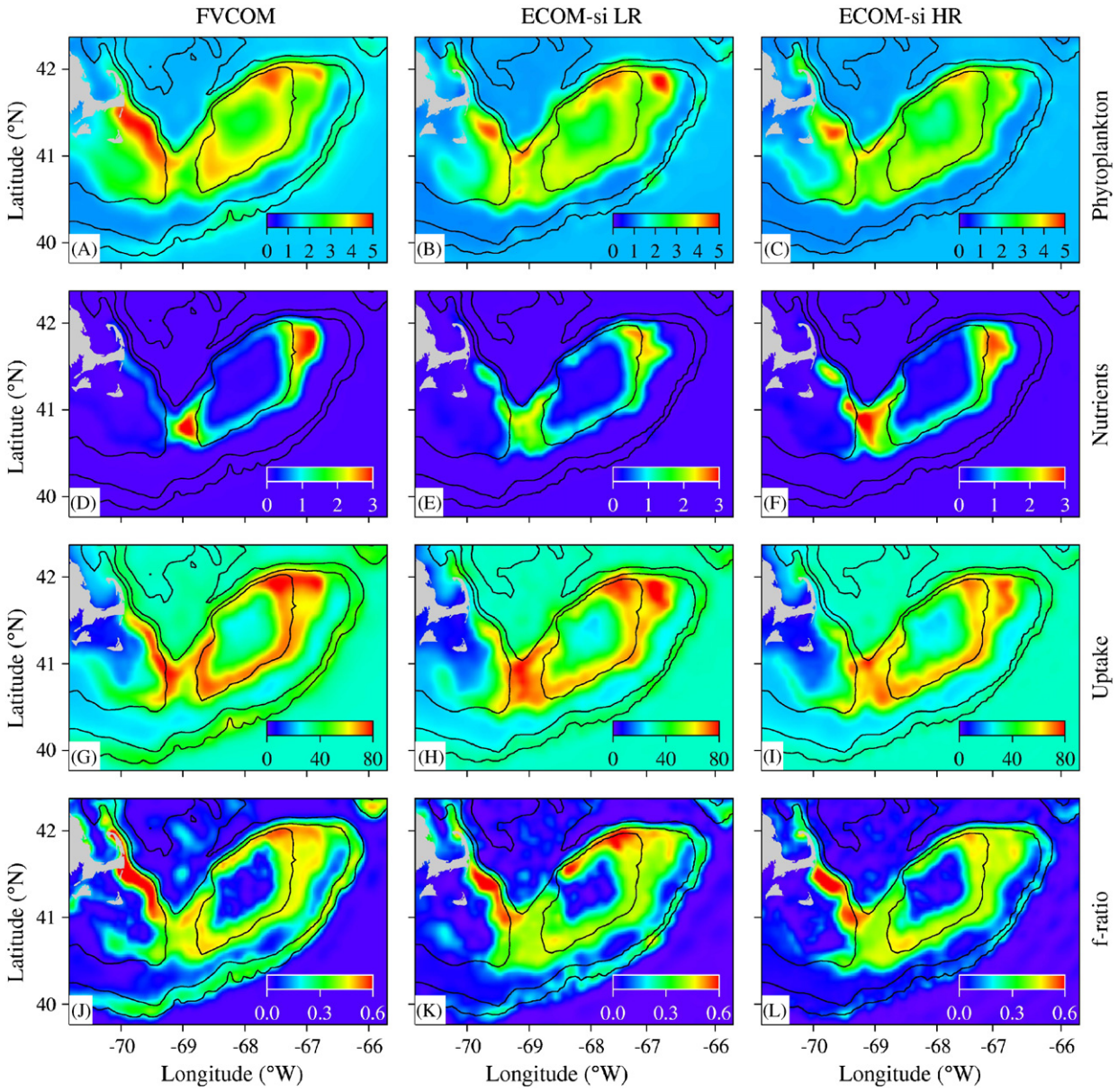

Fig. 5. Simulated distribution of phytoplankton biomass (μmol N l^{-1}), nitrogen concentration (μmol N l^{-1}), nitrogen uptake (mmol N m^{-2} d^{-1}) and *f*-ratio (dimensionless) from the FVCOM (left), "low-resolution" (middle) and "high-resolution" (right) ECOM-si simulations on Georges Bank and over Nantucket Shoals. Phytoplankton biomass and nitrogen concentration were near the surface whereas nitrogen uptake and *f*-ratio values were integrated over the euphotic zone.

water depth was <60 m (Fig. 6). The models also predicted two high biomass phytoplankton patches within the tidal mixing frontal zone on the northern and southern flanks and a subsurface maximum of phytoplankton biomass at a depth of about 25 m below the surface in the stratified region.

In the mixed region on GB where relatively high phytoplankton biomass was simulated, nitrogen was depleted in the entire water column (Figs. 6D–F). On both the northern and southern flanks of GB, the nitricline rose considerably in the stratified region around the slope, forming an upward tongue-like structure of nutrients towards the tidal mixing frontal zone. These patterns were described in detail in the 2D and 3D experiments made by Franks and Chen (1996, 2001).

Both model-predicted nitrogen uptake rate and *f*-ratio showed high values in the surface layer

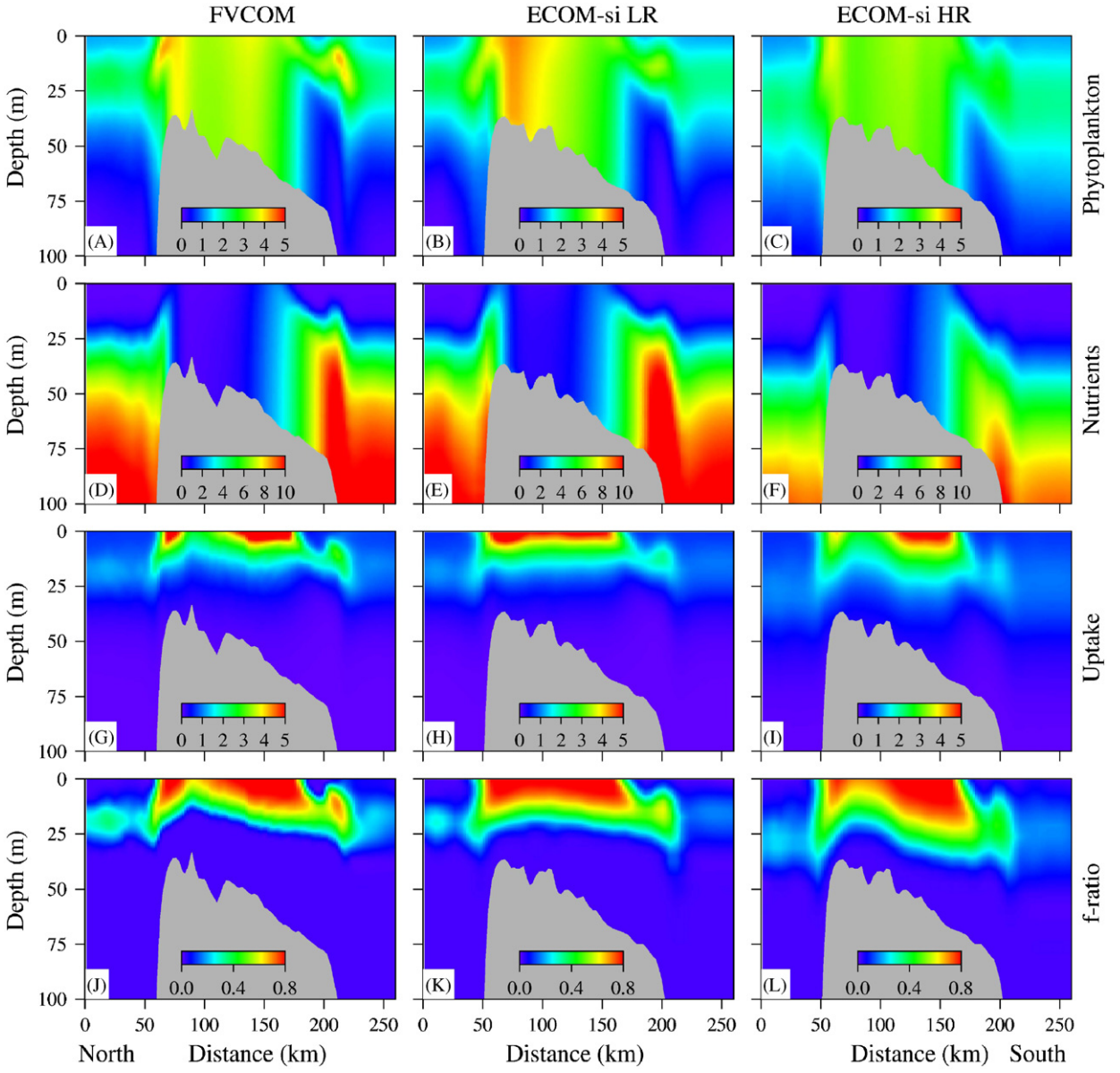

Fig. 6. Cross-bank distributions of simulated phytoplankton biomass (μmol N l^{-1}), nitrogen concentration (μmol N l^{-1}), nitrogen uptake (μmol N l^{-1} d^{-1}) and *f*-ratio (dimensionless) from the FVCOM (left), "low-resolution" (middle) and "high-resolution" (right) ECOM-si simulations. The location of the cross-bank transect is indicated in Fig. 1.

(with a thickness of ~25 m below the surface) on GB, including the shelf break (Figs. 6G–L). This implied that the high phytoplankton biomass throughout the entire water column on the top of GB was produced in the surface layer and was then vertically homogenized due to strong tidal mixing. Nutrient uptake rate and *f*-ratio were high on the bank and decreased off-bank on both the southern and northern flanks, which implied that new production and regeneration essentially occurred on the top of GB around the tidal mixing front.

Although both FVCOM and ECOM-si predicted similar general patterns in the biological fields, significant differences were found in the spatial distribution of phytoplankton and nutrients. On GB, for example, FVCOM tended to predict higher phytoplankton biomass and nutrient concentration on the northern flank and on the northeast peak than did ECOM-si (Figs. 7A, B and D, E). As a

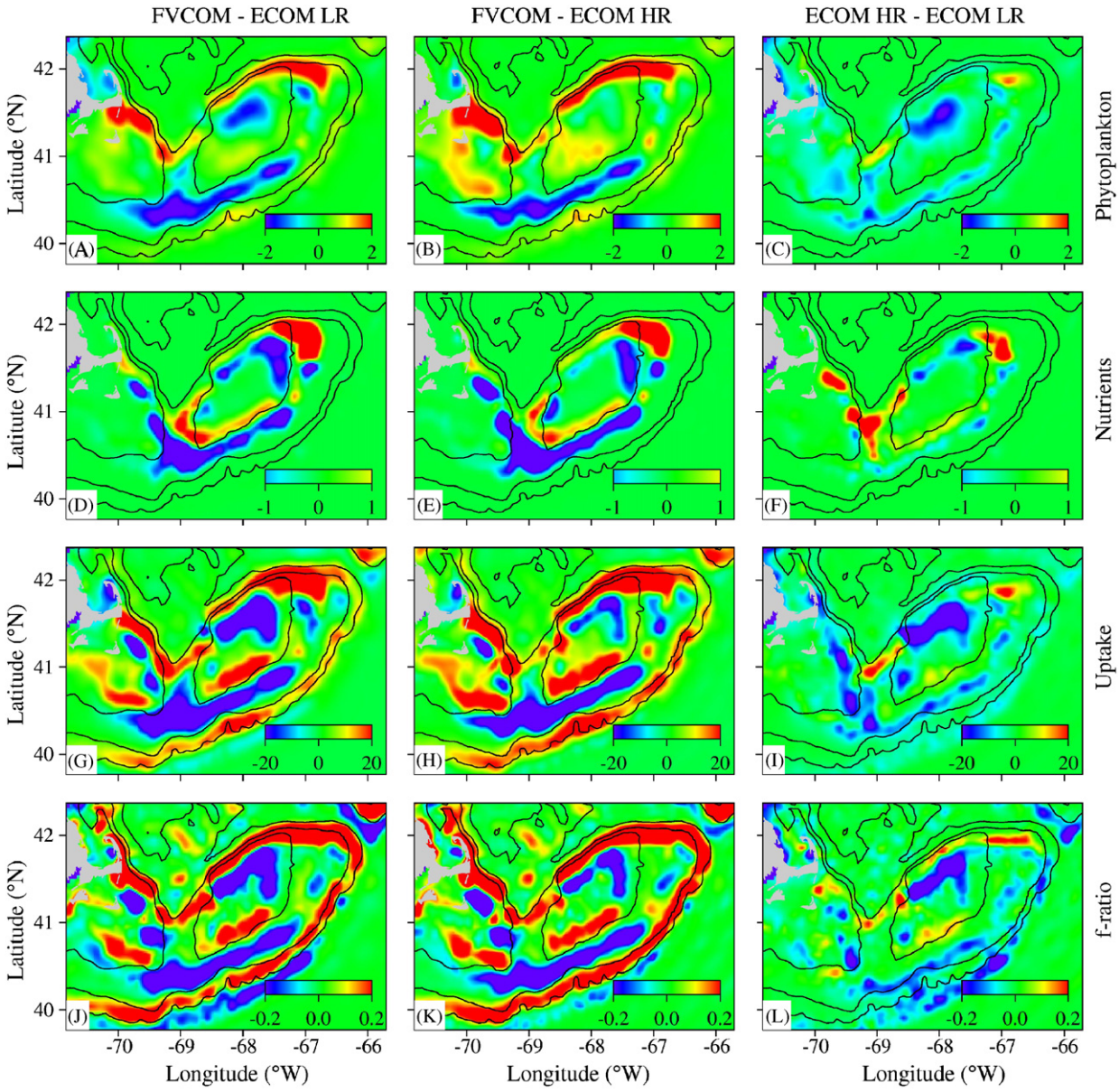

Fig. 7. Differences in phytoplankton biomass (μmol N l^{-1}), nitrogen concentration (μmol N l^{-1}) and *f*-ratio (dimensionless) between the FVCOM and "low-resolution" (left) and "high-resolution" (middle) ECOM-si simulations and between the "high-resolution" and "low-resolution" ECOM-si simulations (right) on Georges Bank and over Nantucket Shoals.

result, FVCOM showed higher nutrient uptake rate and *f*-ratio in these regions than did ECOM-si (Figs. 7G–L). On the other hand, FVCOM showed lower phytoplankton biomass and nutrient concentrations in the mixed region close to the northeast peak of GB than did ECOM-si. The same differences were found along the 60-m isobath over Nantucket Sound and over Nantucket Shoals.

Similar differences were also found in the BF. In the entire inner bay, FVCOM predicted higher phytoplankton biomass than did ECOM-si (Fig. 8). Three patches of high nitrogen concentration were observed in the FVCOM simulation: in the inner bay; around the southern area of Grand Manan Island; and near the southwestern entrance of the BF (Fig. 8D). These three patches were not all captured by ECOM-si. In the low-resolution case, ECOM-si predicted two patches in the southern area of Grand Manan Island and at southwestern entrance of the BF, but not in the inner

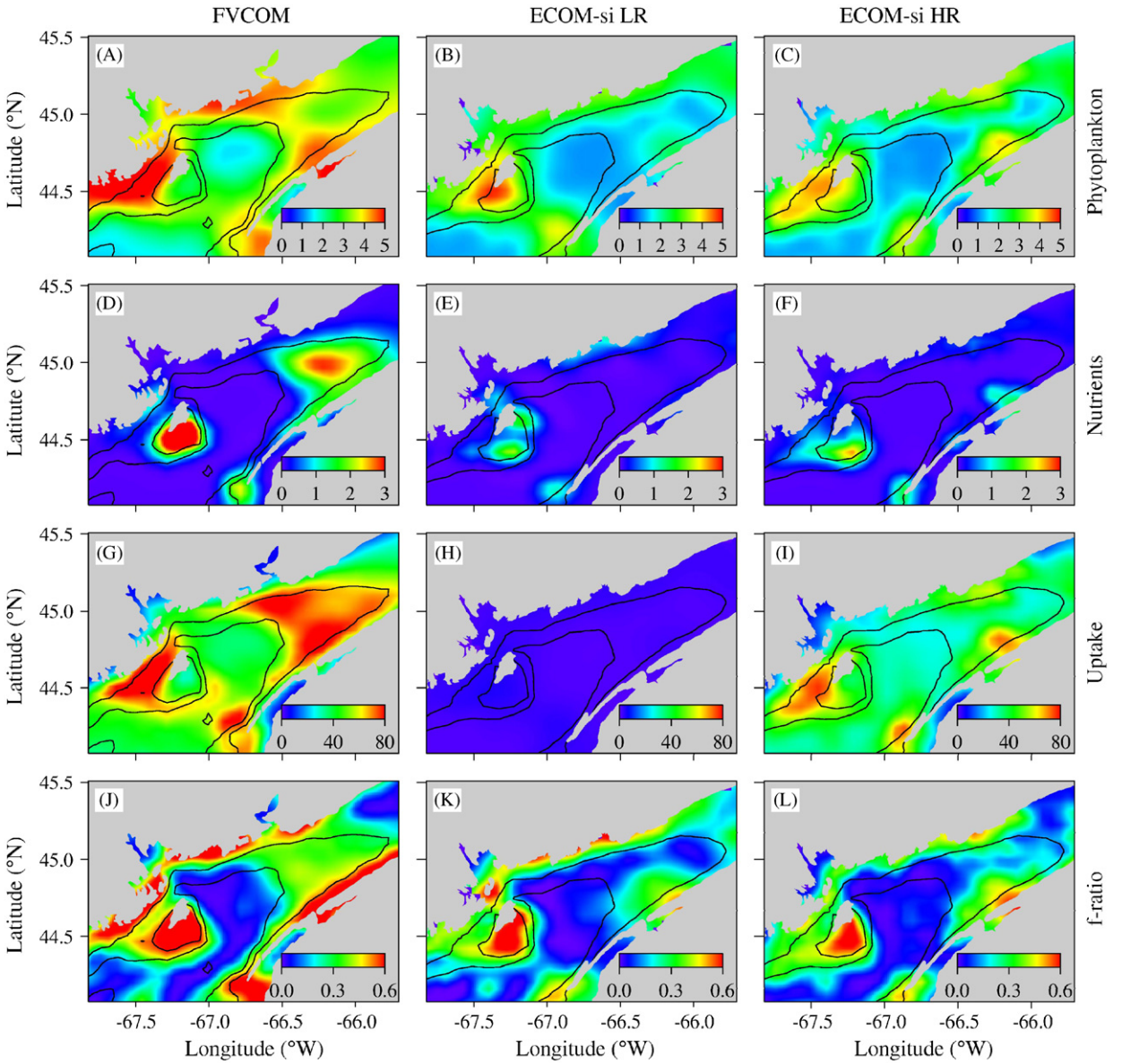

Fig. 8. Simulated distributions of phytoplankton biomass ($\mu mol\,N\,l^{-1}$), nitrogen concentration ($\mu mol\,N\,l^{-1}$), nitrogen uptake ($mmol\,N\,m^{-2}\,d^{-1}$) and *f*-ratio (dimensionless) from the FVCOM simulation (left), "low-resolution" (middle) and "high-resolution" (right) ECOM-si simulations in the Bay of Fundy. Phytoplankton biomass and nitrogen concentration were near the surface, whereas nitrogen uptake and *f*-ratio were integrated over the euphotic zone.

bay (Fig. 8E). When the horizontal resolution doubled, the third patch appeared in the ECOM-si simulation, but it was located closer to the coast and its concentration was lower than the FVCOM solution (Fig. 8F). Correspondingly, FVCOM showed three zones of high nitrogen uptake rate and *f*-ratio in the BF (Figs. 8G and J), but these features were not captured by ECOM-si in the "low-resolution" case (Figs. 8H and K) When the horizontal resolution doubled, ECOM-si seemed to predict similar uptake and *f*-ratio patterns, but the values remained low (Figs. 8I and L). These comparisons suggested that the ECOM-si numerical solution tended to converge toward the FVCOM solution as horizontal resolution increases.

3.2. Experiment B: turbulence model simulations

This experiment compared the results from the coupled FVCOM-NPZ model using different turbulence closure schemes. The model results described here were based on the model runs using the following stability functions: MY2.5, KC, BB, CA and CB. MY2.5 and KC refer to the original and modified MY level 2.5 $q-ql$ turbulence models, while BB, CA and CB refer to the original and modified $q-\varepsilon$ turbulence models. These models were run for the entire computational domain, but the inter-model comparisons were focused on GB only.

For the same given forcing and initial conditions, the $q-\varepsilon$ turbulence models produced much stronger vertical mixing intensity on GB than did the q-ql turbulence models (Fig. 9). The vertically averaged values of eddy viscosity K_M for each case are shown in Fig. 9 (right panels). The distributions of K_M clearly delineated the two groups. The MY 2.5 and KC models predicted similar patterns but significantly different from those produced by BB, CA and CB models. The value of K_M on the northeast peak and in the southern GSC was 30–40% higher in the $q-\varepsilon$ turbulence model simulations than in the $q-ql$ turbulence model simulations. Due to different cutoff values of Richardson number, each model predicted a different vertical distribution of K_M (Fig. 9, left panels). Between the two $q-ql$ turbulence models, KC produced slightly higher mixing intensity in subsurface layers than did MY2.5 in both mixed and stratified regions. Among the $q-\varepsilon$ turbulence models, CA predicted stronger mixing in stratified waters than did BB and CB.

The different intensities of vertical mixing produced by the $q-ql$ versus the $q-\varepsilon$ turbulence model directly affected the simulated results for water temperature, nutrients and phytoplankton on GB (Fig. 10). On the northeast peak of GB and in the GSC, the near-surface water temperature was lower in the simulations of the $q-\varepsilon$ turbulence models (Figs. 10G, J and M) than in the simulations of the $q-ql$ turbulence models (Figs. 10A and D). Correspondingly, nitrogen concentration in these two regions was significantly higher in the cases with BB, CA and CB (Figs. 10H, K and N) than in the cases with MY2.5 and KC (Figs. 10B and E). The maximum difference reached $1.0\,\mu mol\,N\,l^{-1}$. Due to this difference in nutrient supply, the area of high phytoplankton biomass extended off-bank on the northeast peak of GB in the $q-\varepsilon$ model simulations, though the other regions remained very similar in all the cases (Figs. 10C, F, I, L and O).

Selection of different turbulence closure schemes also affected the distributions and values of the uptake rate and f-ratio in the stratified region of GB (Fig. 11). No significant difference was found in the mixed region on the top of GB, but the uptake rate and f-ratio were remarkably different at the outer edge of the frontal zone around the bank and in the stratified region on the northeast peak. Similarly to the distribution of phytoplankton, the area with relatively high uptake rates and high f-ratio extended off-bank in the stratified region on the northeast peak in the $q-\varepsilon$ model simulations compared to the $q-ql$ model simulations. The size of the donut-like ring of high uptake rate and f-ratio was enlarged towards the deep region on the southern flank in the $q-\varepsilon$ model simulations. Due to different intensities of vertical mixing, the values of the uptake rate and f-ratio in some regions on the northeast peak were lower in the simulations with the $q-\varepsilon$ turbulence models than in the simulations with the $q-ql$ turbulence models.

4. Discussion

The fact that FVCOM and ECOM-si have predicted distinctly different distributions of nutrients and phytoplankton in the GoM suggests that the biological simulation can be significantly influenced by model skill. Since FVCOM and ECOM-si present the same dynamics, the difference in the simulated results between these two models is believed to be due to geometric fitting. The flexibility of the unstructured grid used in FVCOM provided a realistic fitting to the coastal geometry and made it possible to build high-resolution meshes along the local isobaths at steep bottom topography. For the same given boundary forcing and initial conditions, FVCOM can provide a more realistic solution than structured grid models in the GoM, particularly on GB and coastal areas. To illustrate this, we conducted a diagnostic analysis by comparing the low- and high-resolution ECOM-si model results with FVCOM in Section 4.1.

The turbulence model study showed a remarkable change in nutrient and phytoplankton concentration due to different mixing parameterizations. This raised a fundamental issue regarding the assessment of biological models used in the GoM. The question here is which turbulence model provided a more realistic mixing profile in this region. To address this

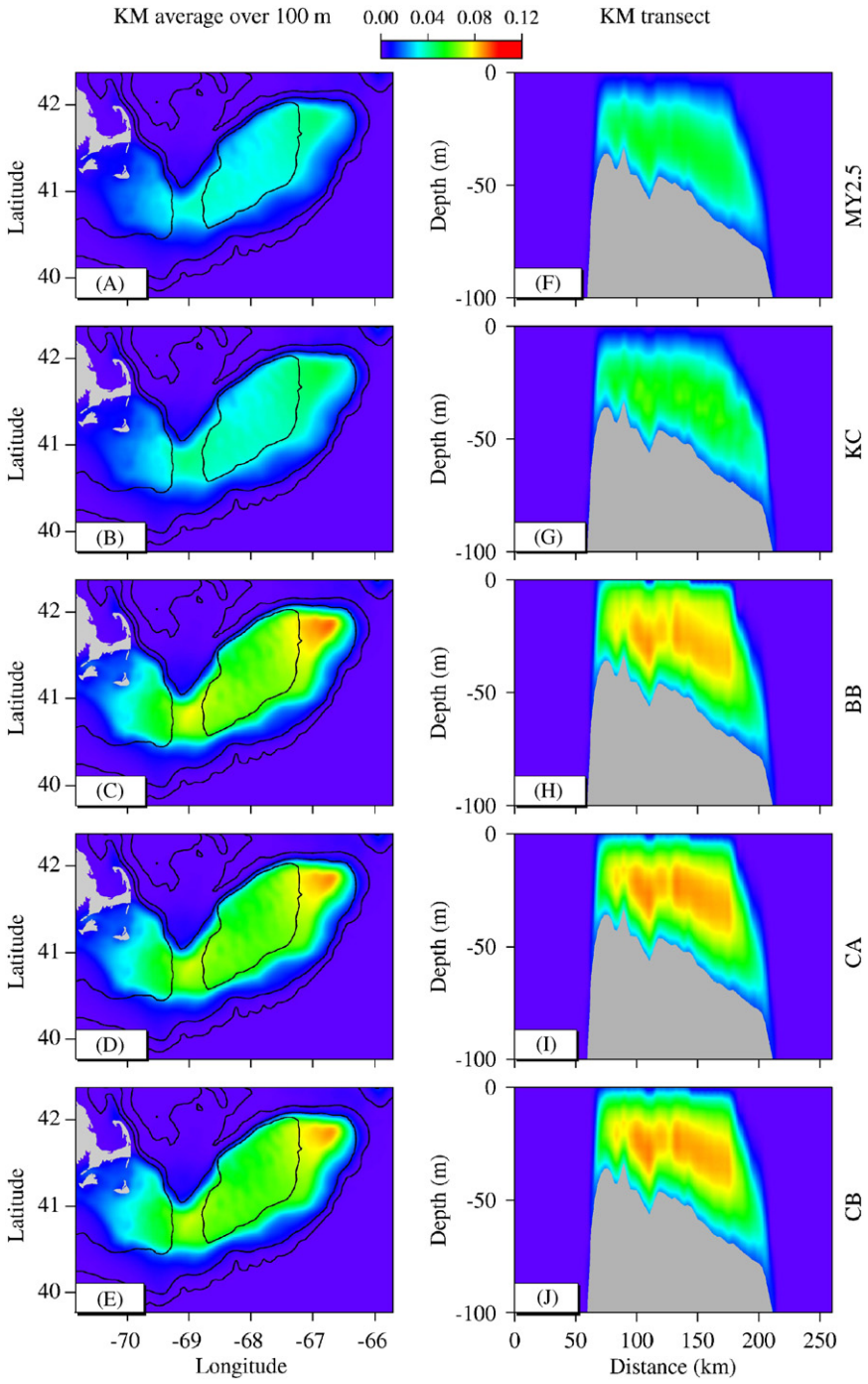

Fig. 9. Distributions of the model-predicted vertical eddy viscosity K_M ($m^{-2}\,s^{-1}$) averaged over the upper 100 m on Georges Bank and in the adjacent regions predicted by MY2.5, KC, BB, CA and CB turbulence closure models (left panels). The cross-bank distributions of K_M predicted by these five models are shown in the right panels.

question, we compared the model-predicted turbulence dissipation rates with field data collected in mixed and stratified regions on GB. A detailed discussion of these results is given in Section 4.2.

4.1. Impacts of geometric fitting

Influences of geometric fitting on the predicted circulation and stratification in the GoM were

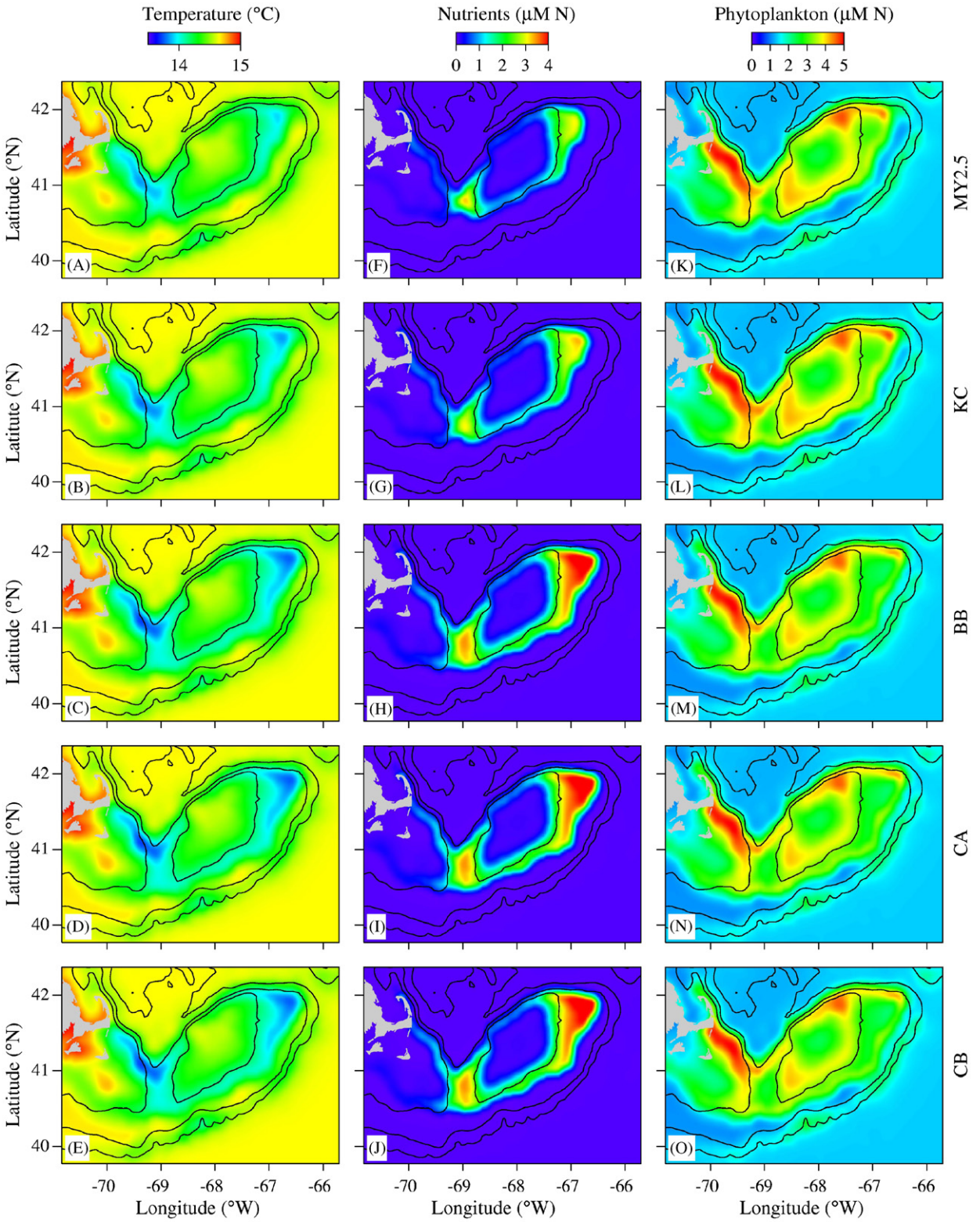

Fig. 10. Simulated surface distributions of temperature (left), nitrogen concentration (μmol N l^{-1}) (middle) and phytoplankton biomass (μmol N l^{-1}) (right) over Georges Bank and in the adjacent regions for the cases with MY2.5, KC, BB, CA, and CB turbulence closure models.

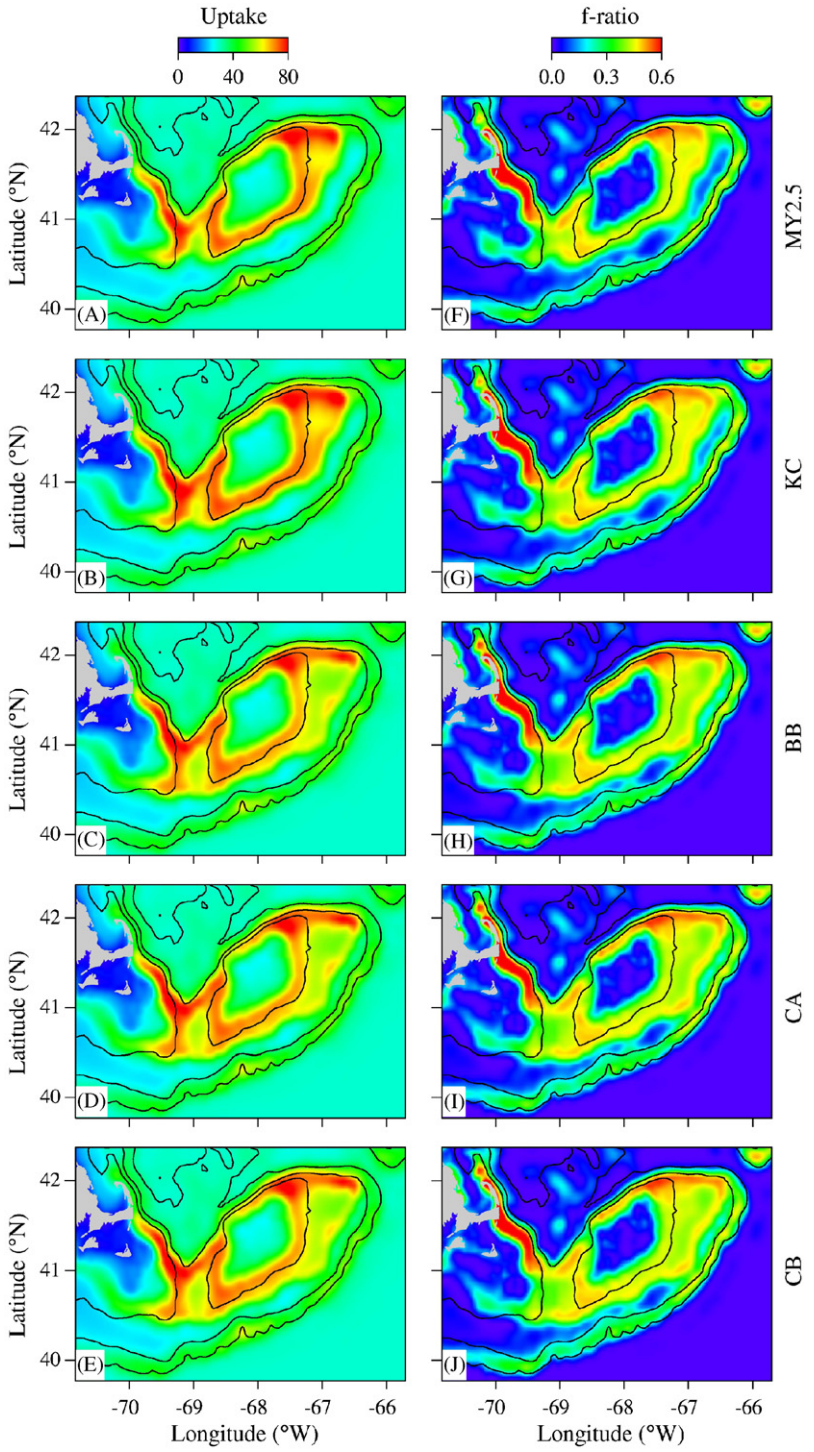

Fig. 11. Simulated distributions of integrated nitrogen uptake over the euphotic zone (mmol N $m^{-2} d^{-1}$) (left) and *f*-ratio over the euphotic zone (right) on Georges Bank and in the adjacent regions for the cases with MY2.5, KC, BB, CA, and CB turbulence closure models.

examined in detail in Chen et al. (2006b). The discussions given herein are focused on three energetic tidal mixing regions: (1) GB, (2) NS, and (3) BF.

4.1.1. Georges Bank

On GB, the distribution of the residual current predicted by FVCOM and ECOM-si differed significantly. On the northern flank, for example, FVCOM predicted a residual current that followed mainly the local isobath, whereas ECOM-si showed a stronger on-bank flow across isobaths (Fig. 12). As pointed out by Chen et al. (2006b), the orthogonal curvilinear grid used in ECOM-si was not built along the local isobath on GB and, as a result, the 3D slope on the northern flank was treated as step-like bottom topography, which can cause a significant on-bank residual current. As the horizontal resolution increased, the on-bank residual flow predicted by ECOM-si was significantly reduced, and the ECOM-si numerical simulation tended to converge to the FVCOM solution. This finding is also applicable to the stratified case shown in the present study. When the horizontal resolution doubled, the ECOM-si-predicted residual current on the northern flank of GB turned significantly in the along-isobath direction (Fig. 12). As illustrated by the cross-bank transects in Fig. 13, the ECOM-si-predicted distributions of water temperature, along-bank residual current and cross-bank residual current differed significantly from the FVCOM results in the "low-resolution' case, but they converged toward the FVCOM solution with the horizontal resolution doubled in the ECOM-si grid.

With high horizontal resolution, FVCOM predicted a stronger along-bank residual current on the northern flank. Stronger tidal-induced upwelling was predicted at the northeast peak where the residual current bifurcated. A patch of high nutrient concentration was generated in the region deeper than 60 m on the northeast peak, which acted as a major nutrient source on GB. This physical mechanism was termed "tidal pumping" in a study carried out by Townsend et al. (2006). In the "low-resolution" grid case, however, ECOM-si predicted stronger on-bank residual flow on the northern flank. Consequently, nutrients on GB were advected in a broader area along the northern flank in the ECOM-si simulation. This is the reason why the ECOM-si-predicted nutrient concentration was higher at the northern edge of the vertically mixed region and also the patch of maximum nutrient

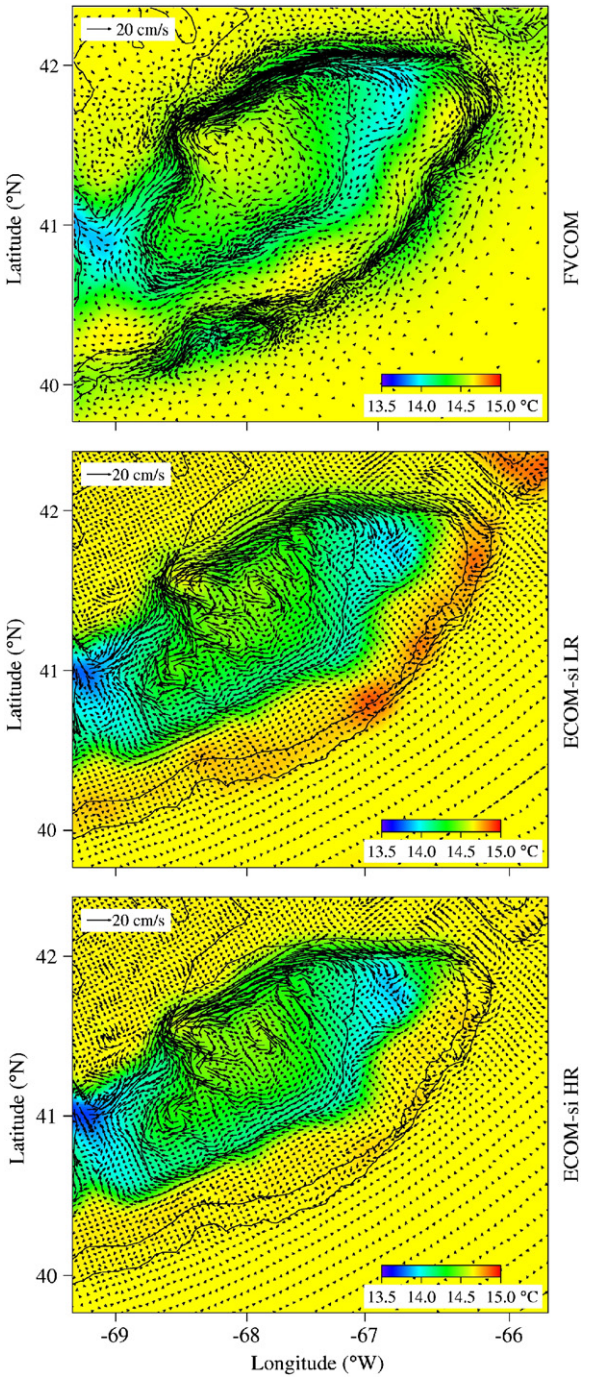

Fig. 12. Distributions of surface residual currents and water temperature from the FVCOM simulation (upper panel), "low-resolution" (middle panel) and "high-resolution" ECOM-si simulation (low panel) on Georges Bank. Solid lines are the 60-, 100- and 200-m isobaths. Currents are depicted at every second grid point in the FVCOM and "high-resolution" ECOM-si simulations to reduce figure burden. Every grid point was included for the "low-resolution" ECOM-si simulation.

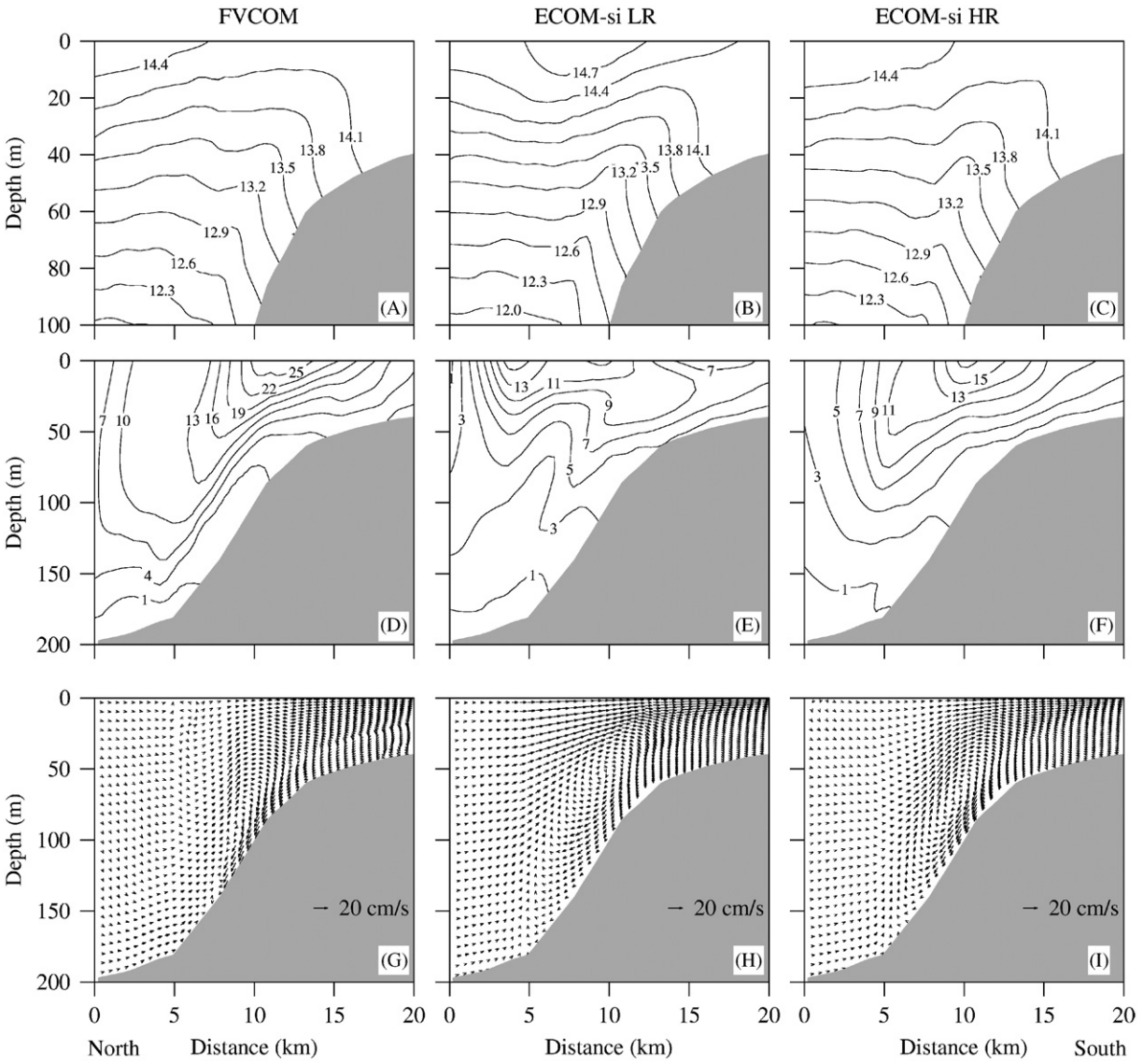

Fig. 13. Cross-isobath distributions of water temperature (A)–(C), along-bank current (D)–(F) and cross-bank current (G)–(I) on the northern flank transect predicted by FVCOM (right), "low-resolution" (middle) and "high-resolution" ECOM-si (right).

concentration shifted toward the 60-m isobath on the northeast peak. With the horizontal resolution doubled, the ECOM-si-predicted residual current on the northern edge of the bank turned significantly in the along-isobath direction, which caused the current splitting point to shift eastward similar to that predicted by FVCOM. Nutrient concentration was significantly reduced at the northern edge of the mixed region, and the patch of maximum nutrient concentration shifted toward deeper regions as in the FVCOM solution. Similar explanations are applicable to the difference in nutrient concentration simulated on the southwestern flank of GB by FVCOM and ECOM-si. Since GB is a nitrogen-limited system, changes in nutrient dynamics directly affected the distribution of phytoplankton, uptake rate, and *f*-ratio.

It should be pointed out that the horizontal resolution around steep bottom topography on GB used in the high-resolution grid of ECOM-si was still lower than that in the FVCOM grid. As the horizontal resolution increases further, ECOM-si's simulation would converge toward the FVCOM solution at the expense of computational efficiency.

This supports our argument that an unstructured grid model with the flexibility in resolving steep bottom topography is more suitable for ecosystem studies on GB.

4.1.2. Nantucket Shoals

In terms of tidal dynamics, Nantucket Shoals (NS) is a transition region between the southern New England shelf to the southwest and the resonant Gulf of Maine to the northeast (Chen et al., 2006a). The tidal-induced residual currents and mixing in that region are controlled by complex physical processes of tidal wave interaction and tidal flushing around Nantucket Island. With detailed representation of the coastal geometry of the island, FVCOM predicted multiple residual eddies around Nantucket Island and a relatively strong clockwise circulation on NS. As a result, a warm-core patch formed inside the clockwise circulation area south of Nantucket Island (Fig. 14, upper panel). As the coastal geometry of Nantucket Island was not adequately represented by the low-resolution grid, ECOM-si did not resolve the tidal-flushing-induced eddies around the island. Although this model did show a clockwise residual circulation on NS similar to FVCOM, the velocity was significantly reduced. The warm water predicted by ECOM-si covered a broader area from Nantucket Sound to NS (Fig. 14, mid-panel). By increasing the horizontal resolution, the simulation result of ECOM-si was improved, particularly in the NS area offshore from Nantucket Island (Fig. 14: lower panel). A distinct clockwise residual eddy appeared on NS, which tended to form a warm-core patch like that in the FVCOM solution. Since even the higher resolution structured grid resolved poorly the complex coastline of Nantucket Island, ECOM-si did not capture the tidal-flushing-induced residual eddies around the island.

The different patterns in currents and eddies predicted by FVCOM and ECOM-si were the key factors in causing the distinct distributions of nutrients and phytoplankton on NS and on the western slope of the GSC. Multiple eddies around Nantucket Island and a large-scale clockwise residual loop current acted like a retention zone of high phytoplankton biomass over NS as shown in the FVCOM simulation (Fig. 5). With the high resolution on the slope, FVCOM predicted high nitrogen uptake rates along the western slope of the GSC and thus generated a high biomass zone in that area. This pattern was partially simulated by

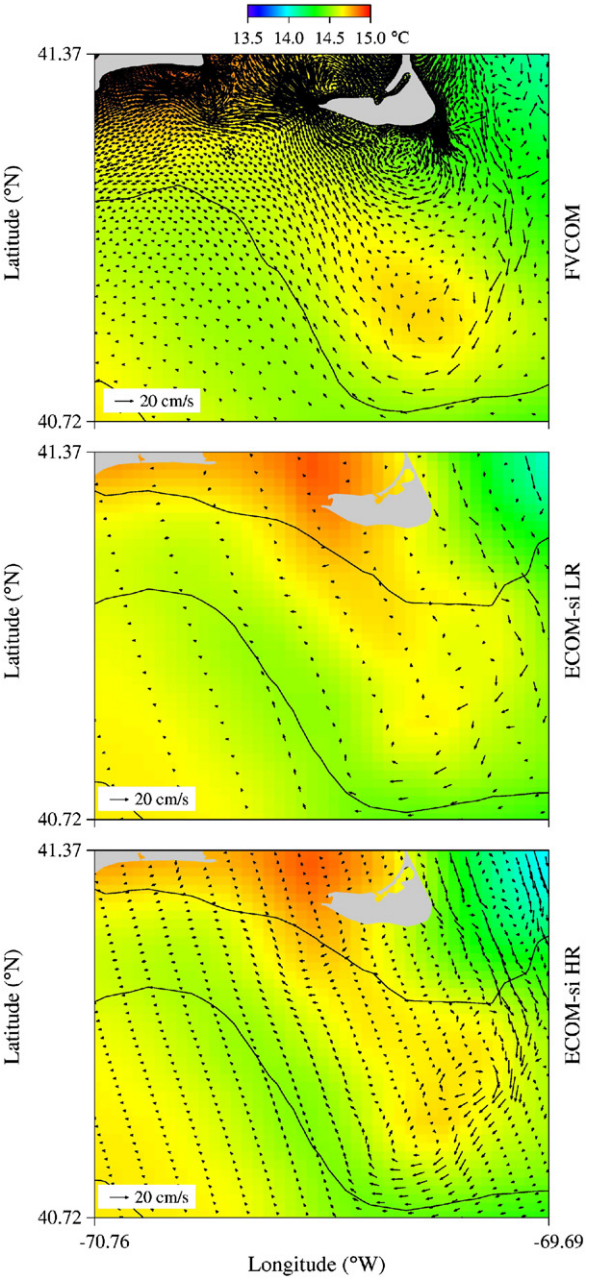

Fig. 14. Surface distributions of residual currents and water temperature predicted by FVCOM (upper panel), "low-resolution" ECOM-si (middle panel) and high-resolution ECOM-si (low panel) over Nantucket Shoals and New England shelf. Solid lines are the 40- and 60-m isobaths.

ECOM-si between the two strong tidal flushing regions around Nantucket Island. This implies that the distribution of phytoplankton in that region is closely related to the strong tidal flushing in Nantucket Sound, which was not adequately

resolved in the structured-grid ECOM-si simulations.

4.1.3. Bay of Fundy

Chen et al. (2006a) examined the impact of coastal geometric fitting on tidal simulation in the BF. With the horizontal resolution used in the present study, FVCOM successfully reproduced the amplitude and phase of the tidal wave in this region. ECOM-si showed a reasonable phase but significantly underestimated the amplitude of the tidal wave. By doubling the horizontal resolution, ECOM-si significantly improved the prediction of tidal amplitude at the sacrifice of an increased phase bias. This finding was supported by comparisons of ECOM-si with an analytic solution for an idealized bay which showed that representation of a curving coastline with a sequence of grid steps can cause significant near-shore phase error even as the step size is reduced (Chen et al., 2006a).

Chen et al. (2006d) also examined the impact of Grand Manan Island on the formation of anticyclonic and cyclonic eddies around the island and a cyclonic eddy in the inner bay of the BF. They suggested that in order to resolve realistically the subtidal circulation in the BF, a model must be capable of resolving the complex coastline of Grand Manan Island and the strong tidal currents in the inner bay.

With adequate matching of the coastline of the BF and Grand Manan Island, FVCOM predicted a pair of anticyclonic and cyclonic eddies in the southern area of Grand Manan Island. A relatively strong cyclonic residual eddy along the 60-m isobath also was resolved (Fig. 15, upper panel). The strong tidal currents predicted by FVCOM resulted in energetic tidal mixing in the inner bay, forming a cold-core area between the 60- and the 100-m isobaths, given the linear distribution of temperature in the initial conditions. These circulation patterns have recently been reported by Sankaranarayanan and McCay (2003), who used a high-resolution model of the BF.

In contrast, the low-resolution grid of ECOM-si could not capture the complex geometry of Grand Manan Island and the coast of the BF. Consequently, ECOM-si resolved only one anticyclonic eddy in the southern area of Grand Manan Island. No cyclonic residual eddy was generated along the 60-m isobath (Fig. 15, middle panel). Because this model significantly underestimated the amplitude of tidal currents and vertical mixing, surface waters remained warmer than that in the FVCOM simulation. With horizontal resolution doubled, the cyclonic residual eddy appeared along the 60-m isobath (Fig. 15, lower panel). With improved simulation of tidal amplitudes and currents, the

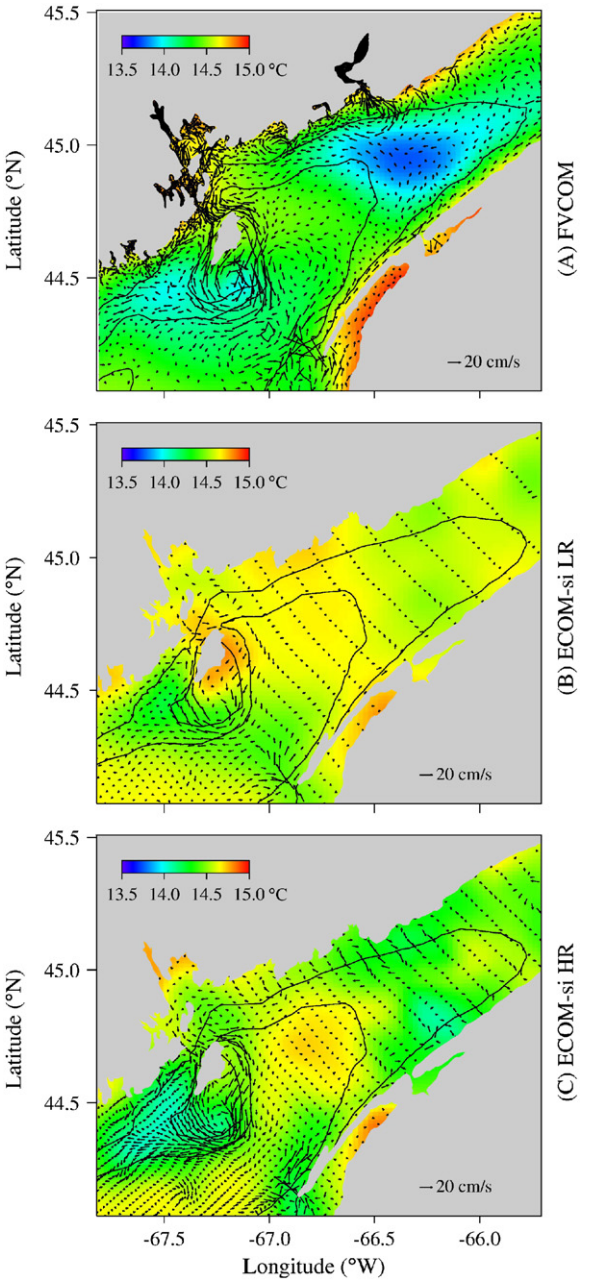

Fig. 15. Surface distributions of residual currents and water temperature predicted by FVCOM (upper panel), "low-resolution" ECOM-si (middle panel) and "high-resolution" ECOM-si (low panel) in the Bay of Fundy. Solid lines are the 60- and 100-m isobaths.

"high-resolution" ECOM-si produced much stronger vertical mixing, which caused the surface water temperature to drop significantly, converging toward the FVCOM results.

The different simulated circulation patterns and tidal mixing intensity can explain the different biological simulations in the BF between the two models. Unlike on GB, increasing horizontal resolution does not resolve the true dynamics in the BF. Due in part to inherent phase errors along a steppy boundary, structured-grid models can not correctly predict the timing of phytoplankton blooms which are closely related to the interaction of tidal currents, river discharge and wind mixing. Although the phase can always be tuned in the local domain of the BF, it can be difficult to adjust in the

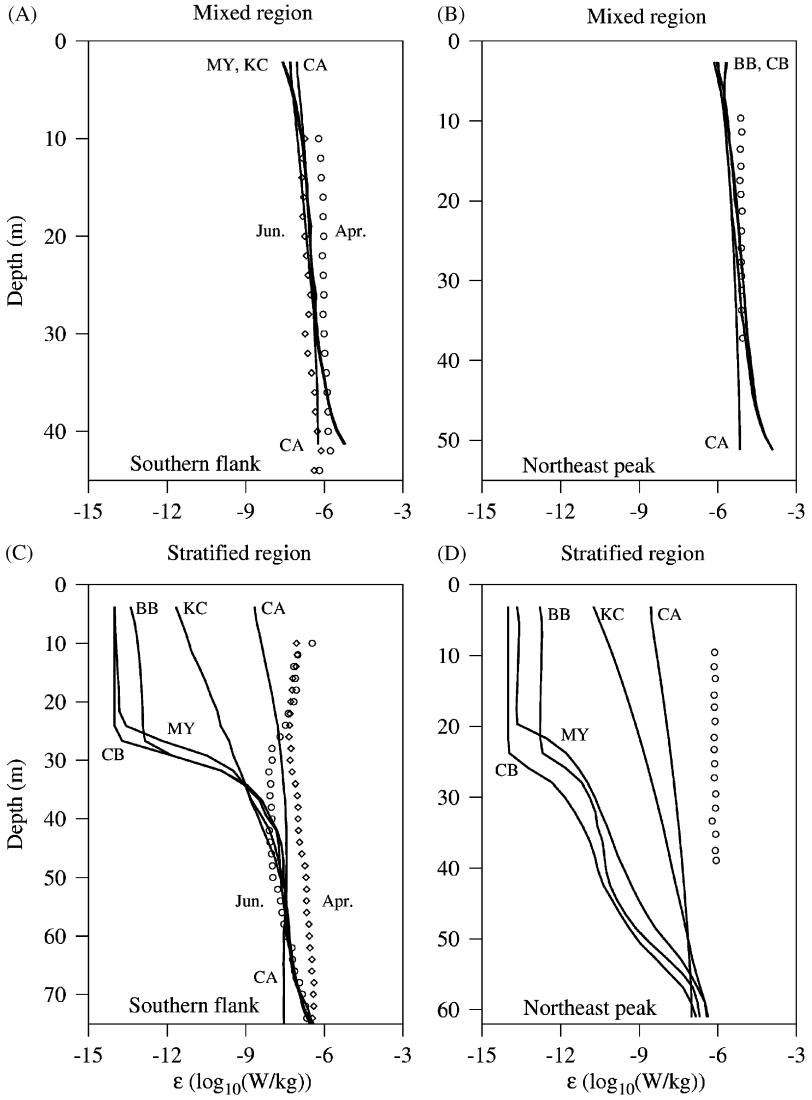

Fig. 16. Comparison between simulated (lines) and observed (symbols) vertical profiles of tidally averaged turbulence kinetic energy dissipation rates at sites A and B in the mixed region and sites C and D in the stratified region on southern and northern flanks of Georges Bank. At site A, the observed vertical profiles represent the averaged values of 17 profiles over 33 h collected in April and 38 profiles over 35 h in June 1995 (Burgett et al., 2001). At site B, the observed profile was constructed by averaging 11 profiles over 9 hours collected on August 2, 1985 (Horne et al., 1996). At site C, the data consisted of 18 profiles over 60 h in April and 78 profiles over 110 h in June, 1995 (Burgett et al., 2001). At site D, the data included 8 profiles over 12 hours collected on August 12, 1985 (Horne et al., 1996). Model-predicted profiles were calculated by time-averaging over the last two tidal cycles. Data at site A and C were provided by D. Hebert (http://globec.whoi.edu/jg/dir/globec/gb/) and data at site B and D were digitized from Horne et al. (1996).

regional domain of the GoM. For this reason, unstructured-grid models are more suitable for this region than structured-grid models.

4.2. Impact of turbulence parameterizations

Chen and Beardsley (1998) made a direct comparison between MY2.5-predicted and observed vertical eddy viscosity on GB and found that MY2.5 produced reasonable vertical profiles of tidal mixing in the mixed region. They also reported that MY2.5 significantly underestimated vertical mixing in the stratified region.

A direct comparison was made in this study between the model-predicted and observed turbulence dissipation rate in the mixed and stratified regions on GB (Fig. 16). The vertical profiles of observed turbulence dissipation rate were based on the microstructure measurements and analysis of Horne et al. (1996) and Burgett et al. (2001). In the mixed region, the vertical profiles predicted by all five turbulence closure schemes were in reasonable agreement with the observed data, particularly for the data collected in June (Fig. 16, upper panel). In the stratified region, however, all the models showed large discrepancies from the observations. On the southern flank, MY2.5, KC, BB, and CB failed to capture the observed turbulence dissipation rate in the upper 30 m, a layer with strong vertical stratification. CA, which had a mixing cutoff at Richardson number of 1.0, showed a reasonable match with the observed profile. On the northern flank where the bottom topography was steep, all the five models underestimated the turbulence dissipation rate. In comparison with the simulations of the other four models, the CA solution was the most similar to field observations.

It should be noted here that the simulation experiments were conducted for an idealized case with linearly-distributed temperature, while the microstructure measurements were carried out in the real environment, which included surface meteorological forcing and hydrographic conditions. Therefore, these model comparison should be interpreted with caution. Because the wind is usually weak on GB during summer, the large discrepancy found between the model-predicted and observed turbulence dissipation rates in the upper stratified layer is unlikely to be accounted for by the lack of the surface wind forcing in the model simulations. It has been recognized that both q–ε and q–ql turbulence closure models tend to underestimate vertical diffusivity in the thermocline (Martin, 1985; Simpson et al., 1996; Burchard et al., 1998). Our comparison suggests that with the inclusion of the five pressure–strain terms, CA had better simulation of the observed turbulence dissipation rate on GB than MY2.5, KC, BB, and CB. This implies that previous modeling efforts based on MY2.5 in this region tended to underestimate vertical mixing, which should be taken into account in future physical and biological modeling in the GoM.

5. Conclusions

Coupled physical and biological model experiments were made to examine the influence of model skill on the temporal and spatial distribution of simulated nutrients and phytoplankton in the Gulf of Maine (GoM). In this study, two critical issues were addressed: (1) geometrical fitting and (2) vertical mixing parameterization. The first issue was studied by running a state-of-the-art Nutrient–Phytoplankton–Zooplankton (NPZ) model with physical fields provided by unstructured-grid, finite-volume coastal ocean model (FVCOM) and structured-grid, finite-difference coastal ocean model (ECOM-si), respectively. The second issue was explored by running a coupled NPZ–FVCOM system with various vertical turbulence modules implemented in the General Ocean Turbulence Model (GOTM). To distinguish these two experiments, we referred to the first as "Experiment A" and the second as "Experiment B".

In Experiment A, inter-model comparisons were focused on three large tidal dissipation regions: Georges Bank (GB), Nantucket Shoals (NS), and the Bay of Fundy (BF). For the same given tidal forcing and initial physical–biological conditions, we found that the ability of a model to accommodate the irregular coastal geometry and steep bottom topography is a critical determinant of its skill in simulating the spatial and temporal structure of N and P.

On GB, with an adequate resolution of the complex 3D geometry of the steep bottom topography, FVCOM reproduced the strong along-isobath residual current jet on the northern flank and current bifurcation on the northeast peak. Tidal-induced strong upwelling in the bifurcation area had direct impacts on the spatial distribution of nutrients and phytoplankton on GB. These features were not captured in the low-resolution simulation

of ECOM-si. Without resolving the 3D slope of steep bottom topography, this model overestimated the on-bank residual current on the northern flank and thus generated different spatial structures of nutrients and phytoplankton as compared with the FVCOM solution. With the horizontal resolution doubled, ECOM-si's simulation began to converge toward the FVCOM solution.

On NS, FVCOM captured the tidal flushing process around Nantucket Island and the residual eddies by resolving the coastlines and bathymetry of Nantucket Island and the rest of Cape Cod. The "low-resolution" ECOM-si did not resolve the major residual eddy fields on NS and around Nantucket Island. With the horizontal resolution doubled, ECOM-si provided a reasonable simulation of the cyclonic eddy on NS but still did not resolve the multiple eddies around Nantucket Island. As a result, the simulated distributions of nutrients and phytoplankton were significantly different between the two models.

In BF, big differences were found in the distribution of nutrients and phytoplankton predicted by FVCOM and ECOM-si. By accurately resolving the coastlines of the BF and Grand Manan Island, FVCOM predicted a pair of anticyclonic and cyclonic residual eddies south of Grand Manan Island and a bay-scale cyclonic residual eddy along the 60-m isobath. These features were not captured by the "low-resolution' ECOM-si. With poor fitting of the complex coastline of the BF and Grand Manan Island, ECOM-si significantly underestimated the amplitude of tidal currents and thus vertical mixing. Increased horizontal resolution in the ECOM-si grid improved the simulation of tidal currents and thus produced stronger vertical mixing. A cyclonic residual eddy along the 60-isobath appeared in the high-resolution simulation of ECOM-si, implying that the numerical solution for the residual current converged toward the FVCOM's solution. Even with the high-resolution grid, the residual flow field around Grand Manan Island remained poorly resolved in the ECOM-si simulation.

Experiment B was focused on the effects of vertical mixing parameterization on GB. Intermodel comparisons were conducted among five selected turbulence closure schemes which represented two types of turbulence closure models: q–ε and q–ql equation models. The results showed that all the turbulence closure models were robust in the mixed region, but not in the stratified region on GB. The model-data comparison suggests that CA, a turbulence closure model with the inclusion of pressure–strain effects from isotropy, shear production, buoyancy production, nonisotropic contribution and vorticity contribution, provided a more realistic vertical profile of the turbulence dissipation rates in the stratified region on GB than the other tested turbulence models. MY2.5, a popular turbulence closure model used in the GoM studies, tends to underestimate the turbulence dissipation rates in the stratified region. The stronger mixing intensity produced by CA has a direct impact on the spatial distribution of nutrients and phytoplankton on GB.

Acknowledgements

The authors thank Drs. Geoffrey Cowles and Qichun Xu for the setup of the physical and turbulence models, Drs. B. Rothschild and K. Stokesbury for encouragement and support in applying the FVCOM-based ecosystem model to the GoM/GB region, D. Stuebe for his help in editing the manuscript and two anonymous reviewers for their constructive comments and suggestions. Special thanks are given to Dr. R. Beardsley who helped us to clean up many scientific bugs and to edit this paper. This study was supported by the research programs of Scallop Fishery Assessment and New England Multispecies Survey at the School for Marine Science and Technology (SMAST), University of Massachusetts Dartmouth, through NOAA Grants DOC/NOAA/NA04NMF4720332 and DOC/NOAA/NA05NMF4721131 and the US GLOBEC/Georges Bank Program through NOAA Grant NA 160P2323 and NSF Grants OCE0227679 and OCE-0234545. The SMAST-UMD contribution number is 06-0701 and the GLOBEC contribution number is 334.

References

Beardsley, R.C., Butman, B., Geyer, W.R., Smith, P., 1997. Physical oceanography of the Gulf of Maine: an update. In: Proceedings of the Gulf of Maine Ecosystem Dynamics Scientific Symposium and Workshop Report 97-1. Reg. Assoc. for Res. in the Gulf of Maine, Hanover, NH, pp. 39–52.

Blumberg, A.F., Mellor, G.L., 1987. A description of a three-dimensional coastal ocean circulation model. In: Heads, N.S. (Ed.), Three-Dimensional Coastal Ocean Models. Coastal and Estuarine Science, vol. 4, pp. 1–16.

Broström, G., 2002. On advection and diffusion of plankton in coarse resolution ocean models. Journal of Marine Systems 35, 99–110.

Burchard, H., Baumert, H., 1995. On the performance of a mixed-layer model based on the κ–ε turbulence closure. Journal of Geophysical Research 100, 8523–8540.

Burchard, H., Bolding, K., 2001. Comparative analysis of four second-moment turbulence closure models for the oceanic mixed lay. Journal of Physical Oceanography 31, 1943–1968.

Burchard, H., Petersen, O., Rippeth, T.P., 1998. Comparing the performance of the Mellor–Yamada and the k–ε two-equation turbulence models. Journal of Geophysical Research 103C, 10543–10554.

Burchard, H., Bolding, K., Villareal, M.R., 1999. GOTM—a general ocean turbulence model. Theory, applications and test cases. Technical Report EUR 18745 EN, European Commission. 231pp.

Burgett, R.L., Hebert, D., Oakey, N.S., 2001. Vertical structure of turbulence on the southern flank of Georges Bank. Journal of Geophysical Research 106C, 22545–22558.

Butman, B., Beardsley, R.C., Magnell, B., Frye, D., Vrmersch, J.A., Schlitz, R., Limeburner, R., Wright, W.R., Moble, M.A., 1982. Recent observations of the mean circulation on Georges Bank. Journal of Physical Oceanography 12, 569–591.

Canuto, V.M., Howard, A., Cheng, Y., Dubovikov, M.S., 2001. Ocean turbulence. Part I: one-point closure model-momentum and heat vertical diffusivities. Journal of Physical Oceanography 31, 1413–1426.

Casulli, V., 1990. Semi-implicit finite difference methods for the two dimensional shallow water equations. Journal of Computational Physics 86, 56–74.

Chen, C.S., 1992. Variability of currents in Great South Channel and over Georges Bank: observation and modeling. Ph.D. Thesis, MIT-WHOI, Boston, 293pp.

Chen, C.S., Beardsley, R.C., 1995. Numerical study of stratified tidal rectification over finite-amplitude of banks. Part I: symmetric banks. Journal of Physical Oceanography 25, 2090–2110.

Chen, C.S., Beardsley, R.C., 1998. Tidal mixing and cross-frontal particle exchange over a finite amplitude asymmetric bank: a model study with application of Georges Bank. Journal of Marine Research 56, 1163–1201.

Chen, C.S., Beardsley, R.C., Limeburner, R., 1995. Numerical study of stratified tidal rectification over finite-amplitude of banks. Part II: Georges Bank. Journal of Physical Oceanography 25, 2111–2128.

Chen, C.S., Beardsley, R.C., Franks, P.J.S., 2001. A 3-D prognostic numerical model study of the Georges Bank ecosystem. Part I: physical model. Deep-Sea Research II 48, 419–456.

Chen, C.S., Liu, L., Beardsley, R.C., 2003. An unstructured grid, finite-volume, three-dimensional, primitive equation ocean model: application to coastal ocean and estuaries. Journal of Atmospheric and Oceanic Technology 20, 159–186.

Chen, C.S., Cowles, G., Beardsley, R.C., 2004. An unstructured grid, finite-volume coastal ocean model: FVCOM User Manual. SMAST/UMASSD Technical Report 04-0601, 183pp.

Chen, C.S., Beardsley, R., Xu, Q.C., Cowles, G., Limeburner, R., 2006a. Tidal dynamics in the Gulf of Maine and New England Shelf: an application of FVCOM. Journal of Geophysical Research, submitted for publication.

Chen, C.S., Huang, H.S., Beardsley, R.C., Liu, H.D., Xu, Q.C., Cowles, G., 2006b. A finite-volume numerical approach for coastal ocean circulation studies: comparisons with finite-difference models. Journal of Geophysical Research, in press, doi.2006jc003458.

Chen, C., Beardsley, R.C., Cowles, G., 2006c. An unstructured grid, finite-volume coastal ocean model (FVCOM) system. Oceanography (Special Issue entitled "Advance in Computational Oceanography") 19 (1), 78–89.

Chen, C., Ji, R., Beardsley, R.C., Davis, C.S., Xu, Q., Lin, H., 2006d. A new high-resolution finite-volume coastal ocean model (FVCOM) for Gulf of Maine: an application on HAB Study. The 2006 Ocean Science Conference, OS11C-5. 20–24 February, Honolulu, HI.

Egbert, G.D., Bennett, A.F., Foreman, M.G.G., 1994. TOPEX/POSEIDON tides estimated using a global inverse model. Journal of Geophysical Research 99, 24821–24852.

Flagg, C.N., 1987. Hydrographic structure and variability. In: Backus, R.H. (Ed.), Georges Bank. MIT Press, Boston, pp. 108–124.

Franks, P.J.S., Chen, C.S., 1996. Plankton production in tidal fronts: a model of Georges Bank in summer. Journal of Marine Research 54, 631–651.

Franks, P.J.S., Chen, C.S., 2001. A 3-D prognostic numerical model study of the Georges Bank ecosystem: Part II: biological–physical model. Deep-Sea Research II 48, 457–482.

Franks, P.J.S., Worblewski, J.S., Flierl, G.R., 1986. Behavior of a simple plankton model with food-level acclimation by herbivores. Marine Biology 91, 121–129.

Galperin, B., Kantha, L.H., Hassid, S., Rosati, A., 1988. A quasi-equilibrium turbulent energy model for geophysical flows. Journal of Atmospheric Sciences 45, 55–62.

Garrett, C., 1972. Tidal resonance in the Bay of Fundy and Gulf of Maine. Nature 238, 441–443.

Garrett, C., 1974. Normal modes of the Bay of Fundy and Gulf of Maine. Canadian Journal of Earth Science 11, 549–554.

Greenberg, D.A., 1979. A numerical model investigation of tidal phenomena in the Bay of Fundy and Gulf of Maine. Marine Geodesy 2, 161–187.

Horne, E.P.W., Loder, J.W., Harrison, W.G., Mohn, R., Lewis, M.R., Irwin, B., Platt, T., 1989. Nitrate supply and demand at the Georges Bank tidal fronts. Scientia Marina 53, 144–148.

Horne, E.P.W., Loder, J.W., Naimie, C.E., Oakey, N.S., 1996. Turbulence dissipation rates and nitrate supply in the upper water column. Deep-Sea Research 43, 1683–1712.

Ji, R., Chen, C.S., Franks, P.J.S., Townsend, D.W., Durbin, E.G., Beardsley, R.C., Lough, R.G., Houghton, R.W., 2006a. Spring bloom and associated lower trophic level food web dynamics on Georges Bank: 1-D and 2-D model studies. Deep-Sea Research, this volume [doi:10.1016/j.dsr2.2006.08.008].

Ji, R., Chen, C.S., Franks, P.J.S., Townsend, D.W., Durbin, E.G., Beardsley, R.C., Lough, R.G., Houghton, R.W., 2006b. The impact of Scotian Shelf Water "cross-over" on the plankton dynamics on Georges Bank: a 3-D experiment for the 1999 spring bloom. Deep-Sea Research, this volume [doi:10.1016/j.dsr2.2006.08.007].

Kantha, L.H., Clayson, C.A., 1994. An improved mixed layer model for geophysical applications. Journal of Geophysical Research 99, 25235–25266.

Limeburner, R., Beardsley, R.C., 1989. CTD observations off New England coast during the South Channel Ocean Productivity Experiment, SCOPEX, June, 1989. Woods Hole Institution Technical Report WHOI-89-52, 252pp.

Loder, J.W., 1980. Topographic rectification of tidal currents on the sides of Georges Bank. Journal of Physical Oceanography 10, 1399–1416.

Loder, J.W., Wright, D.G., 1985. Tidal rectification and front circulation on the sides of Georges Bank. Journal of Marine Research 43, 581–604.

Martin, P.J., 1985. Simulations of the mixed layer at OWS November and Papa with several models. Journal of Geophysical Research 90C, 903–916.

Mellor, G.L., Yamada, T., 1982. Development of a turbulence closure model for geophysical fluid problems. Reviews of Geophysics and Space Physics 20, 851–875.

Moll, A., Radach, G., 2003. Review of three-dimensional ecological modelling related to the North Sea shelf system, Part 1: models and their results. Progress in Oceanography 57, 175–217.

Naimie, A., 1996. Georges Bank residual circulation during weak and strong stratification periods: prognostic numerical model results. Journal of Geophysical Research 101C, 6469–6486.

O'Reilly, J.E., Evans-Zetlin, C.E., Busch, D.A., 1987. Primary production. In: Backus, R.H., Bourne, D.W. (Eds.), Georges Bank. MIT Press, Cambridge, MA, pp. 220–233.

Oschlies, A., 2002. Improved representation of upper-ocean dynamics and mixed layer depths in a model of the north Atlantic on switching from eddy-permitting to eddy-resolving grid resolution. Journal of Physical Oceanography 32, 2277–2298.

Sankaranarayanan, S., McCay, D.F., 2003. Three-dimensional modeling of tidal circulation in Bay of Fundy. Journal of Waterway, Port, Coastal and Ocean Engineering 129, 114–123.

Simpson, J.H., Crawford, W.R., Rippeth, T.P., Campbell, A.R., Cheok, J.V.S., 1996. The vertical structure of turbulent dissipation in shelf seas. Journal of Physical Oceanography 26, 1579–1590.

Smagorinsky, J., 1963. General circulation experiments with the primitive equations, I. The basic experiment. Monthly Weather Review 91, 99–164.

Townsend, D.W., Thomas, M., 2002. Springtime nutrient and phytoplankton dynamics on Georges Bank. Marine Ecological Progress Series 228, 57–74.

Townsend, D.W., Houghton, R.W., Chen, C., Hu, S., Incze, L.S., Lough, R.G., 2006. Modeling studies of cross-isobath nutrient fluxes and biological productivity of Georges Bank. The 2006 AGU Ocean Science Conference, OS34K-06, 20–24 February, Honolulu, HI.